# Exploring the untapped potential of hand-feel soil texture data for enhancing digital soil mapping: Revealing hidden spatial patterns from field observations

Alexandre Eymard, Anne Richer-De-Forges, Guillaume Martelet, Hélène Tissoux, Anne Bialkowski, Marine Dalmasso, Fabrice Chrétien, David Belletier, Guillaume Ledemé, Didier Laloua, et al.

Geoderma 441 (2024) 116769

Contents lists available at ScienceDirect

Geoderma

journal homepage: www.elsevier.com/locate/geoderma

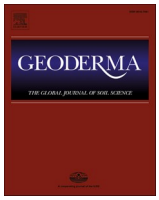

# Exploring the untapped potential of hand-feel soil texture data for enhancing digital soil mapping: Revealing hidden spatial patterns from field observations

Alexandre Eymard [a,b,1], Anne C. Richer-de-Forges [a,1,*], Guillaume Martelet [c], Hélène Tissoux [c], Anne Bialkowski [c], Marine Dalmasso [d], Fabrice Chrétien [e], David Belletier [e], Guillaume Ledemé [e], Didier Laloua [a], Olivier Josière [a], Loïc Commagnac [b], Hocine Bourennane [a], Dominique Arrouays [a]

[a] Info&Sols, INRAE, 45075 Orléans, France
[b] IGN, 33160 Saint-Médard-en-Jalles, France
[c] BRGM, 45060 Orléans Cedex 2, France
[d] IGN, 45290 Nogent-sur-Vernisson, France
[e] IGN, 14200 Hérouville-Saint-Clair, France

ARTICLE INFO

*Keywords:*
Digital soil mapping
Forest topsoils
Hand-feel soil texture
Airborne gamma-ray
Systematic biases
Performance of prediction
Unexpected soilscapes
Soil process knowledge

ABSTRACT

Digital soil mapping (DSM) is commonly conducted using input soil attributes derived from laboratory analyses of geographically referenced samples. Field observations are often abundant and can offer a dense source of soil data that has the potential to enhance DSM predictions. However, they are not widely used due to to concerns about subjectivity and data quality. This study investigates the usefulness of hand-feel soil texture (HFST) data for DSM. We processed HFST data obtained from forest soils in France from two inventory campaigns: (i) HFST determination from systematic 1 km$^2$ grid observations in France utilizing a specialized soil texture triangle, and (ii) HFST observations from soil survey samples, using a different texture triangle. Both sets of HFST data were used as input soil variables, with the same covariates, for predicting topsoil texture In a sizable, forested area through a DSM method. By employing independent sampling and laboratory soil analyses in selected areas, we uncovered measurement bias in one of the datasets. However, intriguingly, these biased observations identified subtle yet highly specific and unexpected patterns of sands in terraces due to alluvial deposits along small rivers. Thus, field soil observations, even if they are biased, should not be dismissed solely based on their overall predictive performance. It is essential to carefully examine predicted maps and covariates to determine whether patterns may have pedological and/or lithological origins and if they are pertinent for enhancing DSM predictions, enhancing soil process understanding, and meeting the requirements of end users. Numerous HFST are available worldwide, these datasets are usually disregarded for DSM. Here we contend that efforts should be put in recovering these data, and their potential for enhancing DSM and deepening our understanding of soil processes.

## 1. Introduction

Digital soil mapping has emerged since the early 1980s' as an appealing, cost-effective, less-subjective method for accelerating the mapping of soil classes or attributes when compared to traditional soil mapping methods (McBratney et al., 2003; Minasny and MCBratney, 2016; Arrouays et al., 2017a). The fundamental premise behind DSM is to posit that soil classes and properties exhibit non-random distributions and can be predicted by establishing empirical relationships between soil information and key factors governing soil formation, such as climate, organisms, relief, parent material, and age. A seminal publication by McBratney et al. (2003) has been a milestone of DSM. These

* Corresponding author.
*E-mail address:* anne.richer-de-forges@inrae.fr (A.C. Richer-de-Forges).
[1] These authors contributed equally to this work.

https://doi.org/10.1016/j.geoderma.2023.116769
Received 15 September 2023; Received in revised form 7 December 2023; Accepted 29 December 2023
Available online 7 January 2024

authors proposed a generic framework called the scorpan-SSPFe (soil spatial prediction function with spatially auto-correlated errors) as a method to produce digital soil maps.

The key advantages and limitations of DSM have been thoroughly discussed in prior works by McBratney et al. (2003), Arrouays et al. (2020a, 2020b), and Ma et al. (2019) and will not be the focus of this paper. Originally developed primarily within academic research, DSM has seen growing adoption and extensive testing over the years, evolving into an operational tool employed across various scales worldwide (e.g. Arrouays et al., 2017a; Chartin et al., 2017; Kamamia et al., 2021; Kidd et al., 2020; Minai et al., 2021; Minasny and McBratney, 2016; Owens et al., 2020; Padarian et al., 2019; Poggio et al., 2021; Sena et al., 2020; Taghizadeh-Mehrjardi et al., 2020, 2019; Taghizadeh-Mehrjardi et al., 2014a; Taghizadeh-Mehrjardi et al., 2014b).

Broad-scale Digital Soil Mapping (DSM) products have been developed worldwide, covering regions, countries, or entire continents (e.g., Chen et al., 2022; Lemercier et al., 2022; Mulder et al., 2016b; Richer-de-Forges et al., 2023a; Tifafi et al., 2018; Vaysse and Lagacherie, 2015). However, detailed soil maps with high resolution for local applications become paramount for informed decision-making. Conventional mapping and soil landscape observations are crucial in refining soilscapes, which are valuable for effective land management. Nevertheless, in many parts of the world, detailed conventional soil mapping faces challenges, primarily due to constraints related to cost. Consequently, there is a pressing need for more detailed local-scale DSM solutions. Achieving this level of detail in DSM is feasible by employing an appropriate combination of soil observations and relevant covariates. This study investigates the effectiveness of a combination of DSM input soil data for mapping soil texture (ST) in a French landscape.

In Digital Soil Mapping (DSM), soil input data are typically derived from laboratory analyses of samples collected from various horizons or fixed layers. However, field observations, such as those related to hand-feel soil texture (HFST), are infrequently utilized, despite their often abundant availability and potential as a dense source of soil data, consequently enhancing DSM predictions (see, for example, Malone and Searle, 2021a, 2021b; Vos et al., 2016).

Across forested soils in mainland France, covering an extensive area of 17.1 million hectares, constituting 31 % of the total mainland France area, a high-density 1 km grid soil observations has been established. This grid includes HFST determinations, resulting in approximately 190,000 auger descriptions that have recently been integrated into the French national soil information system. Notably, the first campaign has already covered all forested soils in mainland France, encompassing around 171,000 data points, and the second campaign is currently underway. This presents a significant opportunity with the potential to substantially enhance DSM predictions of soil texture (ST), specifically within forest soils.

In this study, we explore the usefulness of HFST data for DSM of soil texture class on a French 'département' (French départements are administrative districts with average areas of approximately 5,500 km$^2$). This study investigated low-cost, high-density HFST information collected from soil descriptions of two programmes:

- One programme was the conventional mapping of the 'Loiret' département at a scale of 1:250,000 (Richer-de-Forges, 2008; Richer-de-Forges et al., 2008). Soil surveyors conducted a purposive sampling. Soil pits and several additional soil auger borings were gathered. This programme is conducted by the French national soil survey framework [Inventaire, Gestion et Conservation des Sols (IGCS)].
- The second programme was a systematic forest inventory conducted by the French National Institute of Geographic and Forest Information (IGN). The sampling was unaligned, involving one observation point selected randomly in each cell of the 1 km$^2$ grid as described above (Cluzeau and Drapier, 2001).

An airborne gamma-ray spectrometry map was used as a covariate to obtain soil information down to approximately 60 cm (Minty, 1988; Rawlins et al., 2012, 2007; Reinhardt and Herrmann, 2019).

The aim of this study was to answer the following questions:

- Does HFST provide beneficial information as an input variable in DSM?
- Are two independent HFST datasets comparable or complementary?
- Can airborne gamma-ray spectrometry detect specific local soil properties?
- Can DEM derivatives help predict and explain specific soil texture patterns?
- Does combining different HFSTs datasets and the covariates cited above into a DSM framework enable mapping soilscapes with specific properties?

## 2. Material and methods

### 2.1. Study area

The study area was located in the Loiret département within the French Centre-Val de Loire region (Fig. 1). Forest soils were the focus of this study.

Loiret covers an area of 677,000 ha. The relief is flat, with an average elevation of 100 m.a.s.l., ranging from 273 to 66 m. The area has a 'degraded oceanic' climate with mild winters and cool summers. However, this climate has changed slightly, with an increasing frequency of hot and dry summers. The average annual temperature is approximately 11 °C (30 y average), and the total annual precipitation ranges between 600 and 700 mm (Joly et al., 2010). Loiret is crossed by the Loire River, the longest river in mainland France.

Forests cover approximately 31 % of the department (210,000 ha) and are primarily divided into two large massifs: the national forest of Orléans, north of the Loire River, and the Sologne, south of the Loire River. The soils of Loiret show high spatial variability owing to the great diversity of lithology and derived parent materials (Horemans, 1962; Lacquement et al., 2015; Liard et al., 2017; Macaire, 1985; Martelet et al., 2013; Richer-de-Forges et al., 2008; Tissoux et al., 2017). The primary soils observed under forest vegetation are Arenosols, Fluvisols, Colluviosols, Luvisols, and Planosols; some Cambisols and Vertisols are also observed on clayey parent materials (Richer-de-Forges et al., 2008). More locally impervious clayey subsoils located in depressions can lead to the development of Gleysols and Histosols (Zocatelli et al., 2014).

This study evaluated the prediction topsoil (see the definition of topsoil that we used in section 2.2.) texture by DSM using two different soil datasets and common covariates for forest soils in the entire département. We then focused on a more detailed area in Sologne to better explain and evaluate differences between the two DSM predictions (Fig. 1).

### 2.2. Soil information

Section 2.2 describes the soil information retained as learning variables for DSM.

In the sections 2.2.1 and 2.2.2 soil information were extracted from the existing databases. Topsoil was defined as the surface organo-mineral horizon (excluding O horizons). This horizon was nearly always a A horizon and was always thicker than 20 cm.

#### 2.2.1. Profiles and auger borings used for the initial 1:250,000 soil map

A 1:250,000 soil map of Loiret was obtained by a conventional soil survey using free and purposive sampling. Data were acquired by several organisations [primarily the National Research Institute for Agriculture, Food and the Environment (INRAE) and the Chambre d'Agriculture du Loiret] in the framework of two primary programmes: (i) the systematic 1:250,000 soil inventory of France and (ii) the systematic 1:50,000 soil

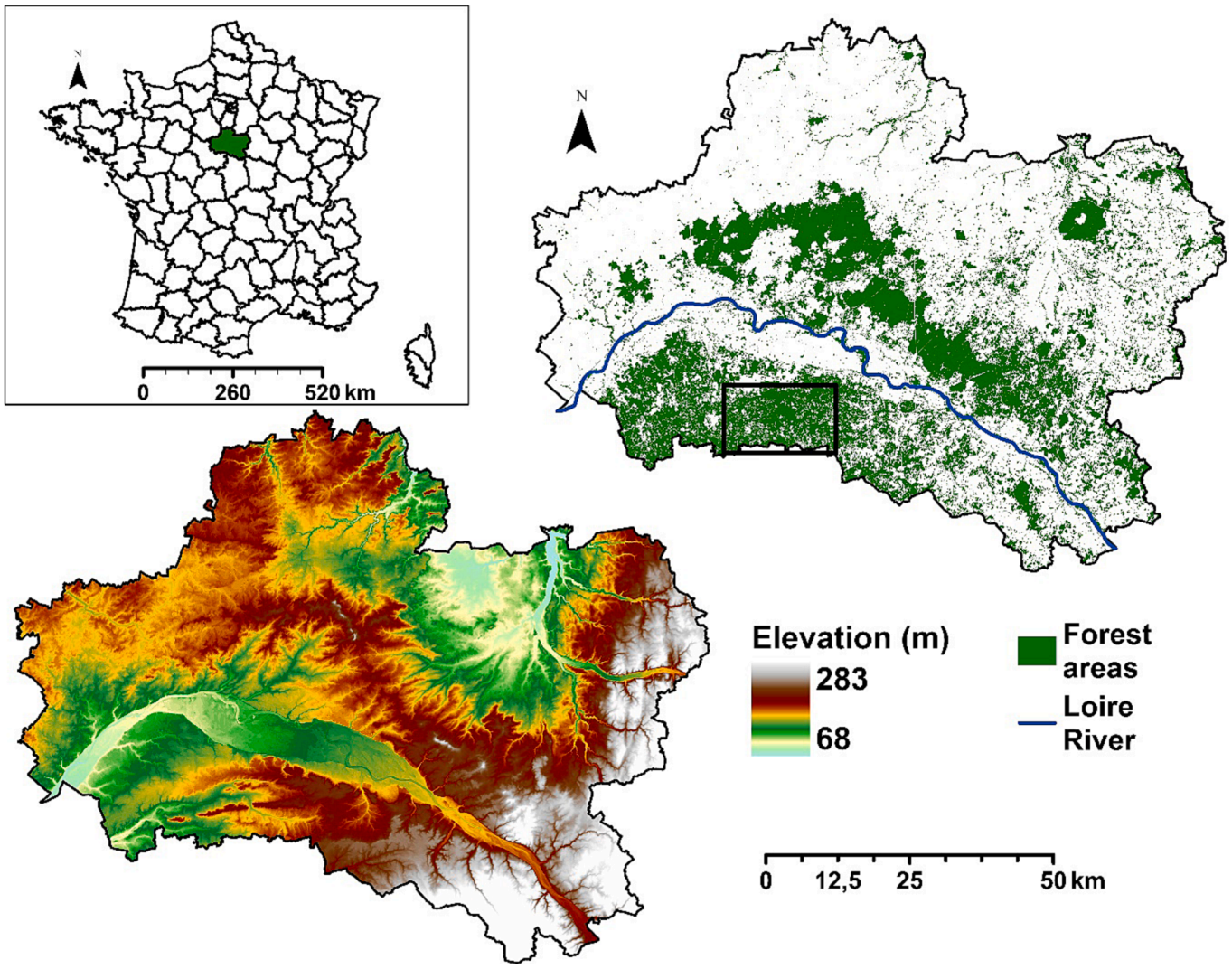


**Fig. 1.** Location of the study area; top left: Mainland France and the Loiret département (in green); bottom left: elevation; right: forested areas in the Loiret département (in green) and the location of an independent probability sampling study in the Sologne area (black rectangle).

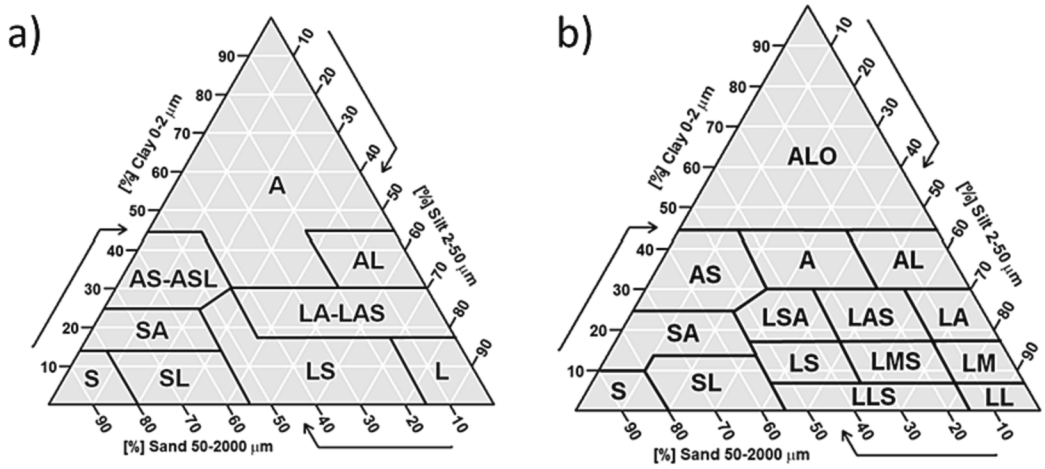


**Fig. 2.** Texture triangles used for the two inventories. a) IGN and b) IGCS triangles. Some textures are the same (AS-ASL and AS, and AL and AL). Other textures are different and correspond (i) to some IGCS textures grouped into IGN textures (LL + LM IGCS = L IGN; ALO + A IGCS = A IGN) or (ii) to grouping and changes in limit values. Tentative translation of the ST class names in English: ALO: heavy clay, A: clay, AL: silty clay, AS: sandy clay, ALS: sandy-silty clay, LA: clayey silt, LAS: sandy clayey silt, LSA: clayey sand silt, SA: clayey sand, S: sand, SL: silty sand, LL: silt, LS: sandy silt, LMS: sandy medium silt, LM: medium silt, LLS: sandy silt. Note that the classes and names are different from the USDA (United States Department of Agriculture) triangle.

mapping of Loiret.

All soil surveyors were experienced and used the same protocols and a standard texture triangle to describe the soils in the field. The 'Aisne' triangle defined by Jamagne (1967) was used, and encoded in the 'soiltexture' package in R software (Moeys et al., 2018). The triangle is hereafter named the 'IGCS triangle', as it was the only triangle that was used in Loiret, and to avoid confusion because 'Aisne' is also the name of another French département (Fig. 2). The data stored in the national database included, among others, the depths, names, horizons, as well as their HFST.

Because topsoil texture was the primary interest of this study, we retained the HFST and depth of the first organo-mineral horizons and recorded the depth of change in HFST and the new ST class when observed at deeper depths.

#### 2.2.2. Mini-pits and auger borings from the systematic forest soil inventory

The systematic forest soil inventory is a national programme conducted by the 'Institut National de l'Information Géographique et Forestière' (IGN). This program aims to cover all forests in France following a systematic unaligned sampling based on a 1 $km^2$ grid. In each forested area of France, one point was randomly selected within a 1 $km^2$ cell. A mini-pit of 0.4 × 0.4 × 0.4 m was dug and described, and an auger boring was performed deeper (up to 1 m depth, or less if the soil was shallower), both with a description of the names, depth, and HFST of the horizons. The ST triangle used by IGN (hereafter named the 'IGN Triangle') differed from the 'IGCS triangle' (Fig. 2). For IGCS, we retained the HFST of the upper mineral horizons of the topsoil and recorded their thickness and the new ST class when observed at deeper depths.

#### 2.2.3. Sampling design and density differences between the two datasets

In forest soils, the total number of sampled points was 1,908 and 1,988 for IGCS and IGN, respectively. Note that the spatial distributions of the sampling points were different (Fig. 3).

The sampling design for the IGN data was based on a systematic unaligned grid, resulting in a regular sampling density. In contrast, the sampling density for the IGCS soil map was more clustered, because the IGCS database included some close observations from studies conducted at scales more detailed than 1: 250,000 (see for example the red rectangle in the middle of the Loiret). Conversely in many areas, the IGCS soil observations were less dense than those conducted by IGN. This is partly due to the fact that IGCS sampling mainly came from free survey. The knowledge and efficiency of the soil surveyor enabled him/her to reduce the sampling density and to choose locations according to mapping purpose. Conversely, when a soil surveyor suspected that spatial changes occured, he/she densified sampling to better capture the limits between soil mapping units.

In regions like Sologne, located to the south of the département, accessing certain areas posed challenges, as most of the forests were privately owned properties. In contrast to surveyors from INRAE and Chambres d'Agriculture, IGN surveyors had the advantage of an official decree allowing them to enter these areas and designate specific points they intended to visit. Consequently, they could schedule their observations by appointment, a convenience not afforded to soil surveyors conducting free surveys, who often had unplanned sampling locations.

### 2.3. Covariates for DSM

Table 1 lists the covariates used to run the DSM predictions for the ST classes.

#### 2.3.1. DEM derivatives

The Digital Elevation Model (DEM) employed in this study has a cell resolution of 25 m and an elevation resolution of 1 m, which is a product of IGN. We utilized this DEM both as the source for raw elevation values and for calculating a range of terrain derivatives. Aspect is a circular variable. Aspect was transformed into two variables, sinφ and cosφ, as recommended by Mardia (1972) and Batschelet (1981). This transformation is widely used in soil science (e.g. King et al., 1999; Bourennane et al., 2000) when the slope aspect derived from a digital elevation model is considered in modeling soil variables. Additionally, we computed focal mean and focal standard deviations of elevation for each pixel, along with selected derivatives, across multiple windows of increasing size (specifically, with radii of 100, 500, and 1000 m), a methodology consistent with the approaches of Grinand et al. (2008) and Chen et al. (2021). These calculations were performed individually for each pixel, yielding DEM derivatives associated with various scales of spatial variation.

#### 2.3.2. Airborne gamma-ray spectrometry data

Airborne gamma-ray spectrometry data are commonly used to map regolith and soil properties. A review by Reinhardt and Herrmann (2019) provided an overview of the possibilities offered by this technique for directly or indirectly mapping numerous soil properties.

An airborne gamma spectrometry survey was conducted in 2009 (Terraquest LTD, 2009). The flights were undertaken at an elevation of 80 m along a regular flight path consisting of flight lines spaced 1 km apart in the N-S direction and perpendicular tie-lines spaced 10 km apart. Along the flight lines, data were recorded with an RS 500 NaI

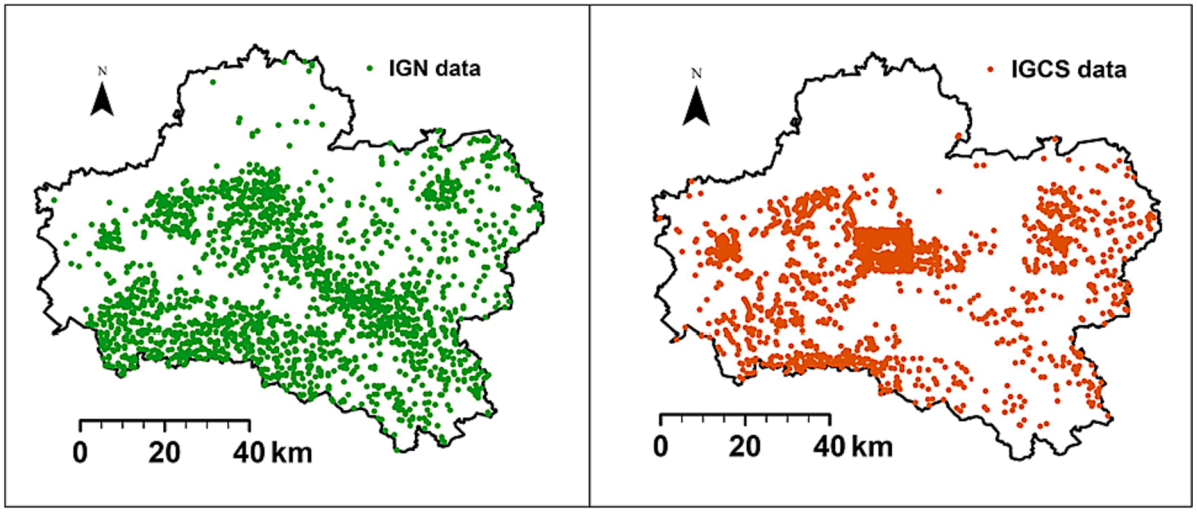


**Fig. 3.** The density of soil observations for the two sampling designs. The IGN is shown in green, and the IGCS is shown in red.

**Table 1**
Covariates used for digital soil mapping.

| Abbreviation | Description | Unit | Reference |
|---|---|---|---|
| DEM | Elevation | m | DEM (IGN, 2011)[1] |
| DEM100M | Focal mean of elevation within a 100 m radius | m | DEM (IGN, 2011) |
| DEM100S | Standard deviation of elevation within a 100 m radius | m | DEM (IGN, 2011) |
| DEM500M | Focal mean of elevation within a 500 m radius | m | DEM (IGN, 2011) |
| DEM500S | Standard deviation of elevation within a 500 m radius | m | DEM (IGN, 2011) |
| DEM1kmM | Focal mean of elevation within a 1 km radius | m | DEM (IGN, 2011) |
| DEM1kmS | Standard deviation of elevation within a 1 km radius | m | DEM (IGN, 2011) |
| Exp | Aspect | sinφ and cosφ | DEM (IGN, 2011) |
| dppr | Distance from the nearest drainage network | m | DEM (IGN, 2011) |
| beven | Beven index, also named the Topographic wetness index (TWI). TWI is equal to: ln(*a*/tan *b*), where *a* is the local upslope area draining through a certain pixel. | m | DEM (IGN, 2011) |
| CURV_M | Mixed curvature | m | DEM (IGN, 2011) |
| CURV_V | Vertical curvature | m | DEM (IGN, 2011) |
| CURV_H | Horizontal curvature | m | DEM (IGN, 2011) |
| Slp100M | Focal mean of slope within a 100 m radius | degree | DEM (IGN, 2011) |
| Slp100S | Standard deviation of slope within a 100 m radius | degree | DEM (IGN, 2011) |
| Slp500M | Focal mean of slope within a 500 m radius | degree | DEM (IGN, 2011) |
| Slp500S | Standard deviation of slope within a 500 m radius | degree | DEM (IGN, 2011) |
| Slp1kmM | Focal mean of slope within a 1 km radius | degree | DEM (IGN, 2011) |
| Slp1kmS | Standard deviation of slope within a 1 km radius | degree | DEM (IGN, 2011) |
| litho | Lithology classified into seven covariates and in a binary code (1, 0) | Binary: 1 = presence; 0 = Absence | BRGM (Giot, 2002) |
| U | Uranium (interpolated from airborne gamma-ray spectrometry emissions) | ppm (mg/kg) | BRGM (Martelet et al., 2014) |
| K | Potassium (interpolated from airborne gamma-ray spectrometry emissions) | g/100 g | BRGM (Martelet et al., 2014) |
| Th | Thorium (interpolated from airborne gamma-ray spectrometry emissions) | ppm (mg/kg) | BRGM (Martelet et al., 2014) |
| TOT | Gamma-ray total count (interpolated from airborne gamma-ray spectrometry emissions) | nGy/h | BRGM (Martelet et al., 2014) |
| K/Th | Ratio between K and Th (interpolated from airborne gamma-ray spectrometry emissions) | / | BRGM (Martelet et al., 2014) |
| K/U | Ratio between K and U (interpolated from airborne gamma-ray spectrometry emissions) | / | BRGM (Martelet et al., 2014) |
| Th/U | Ratio between Th and U (interpolated from airborne gamma-ray spectrometry emissions) | / | BRGM (Martelet et al., 2014) |

NB: The seven lithological units are grouped as follows: *1) alluvial deposits, 2) silex and chalk, 3) marl, 4) limestone, 5) sand, 6) silt, and 7) silty clay.*
[1]Extracted from https://geoservices.ign.fr/bdalti.

spectrometer (including two detectors of 50.4 l observing downward and 8.4 l observing upward) at an interval of 1 s (i.e. approximately one spectrum every 70 m) with a footprint of each measurement of approximately 150 × 300 m. Each data point consisted of a 512-channel energy spectrum ranging from 0.4 to 3.0 MeV. The total count (absorbed dose rate in nanogray/h) and concentrations of uranium (ppm), thorium (ppm), and potassium (%) were derived from the raw spectra following International Atomic Energy Agency (IAEA) processing guidelines (IAEA, 2003, 1991), including corrections related to the presence of atmospheric radon, cosmic background, or the Compton effect, as well as attenuations related to variations in altimetry. The corrected gamma-spectrometric data were then interpolated by the Bureau de Recherches Géologiques et Minières (BRGM) on regular 250 m cell grids using a standard minimum curvature interpolator.

Airborne gamma spectrometry data provides information on uranium, thorium, and potassium content of approximately the upper 60 cm of the soil (Minty, 1997). In a review, Reinhardt and Herrmann (2019) indicated a depth range of 30–60 cm for non-organic soils. For more details regarding the use of gamma spectrometry for mapping, we referred to the studies by Wilford (2002) and Wilford and Minty (2006) and to the review from Reinhardt and Herrmann (2019).

This airborne gamma-ray spectrometry survey had already been used to refine lithology, regolith, and certain soil property maps in various parts of the Centre-Val de Loire region, including Loiret (e.g. Chen et al., 2021; Lacquement et al., 2015; Liard et al., 2017; Martelet et al., 2013; Tissoux et al., 2017).

#### 2.3.3. *Final resolution of the covariates*

All covariates defined above were resampled to a 90 × 90 m cell grid according to the specifications of *GlobalSoilMap* (Arrouays et al., 2014a; Arrouays et al., 2014b).

### 2.4. *DSM and global assessment of performances*

We independently predicted topsoil ST classes using the two soil observation datasets described above but with the same set of covariates (Table 1). Our objectives were (i) to predict the topsoil texture for each forested pixel using two different learning datasets gathered in the field and (ii) to compare the predictions.

We used Random Forest (Breiman, 2001), which is among the most frequently used machine learning tools in DSM (Chen et al., 2022; Heung et al., 2016; Padarian et al., 2019). Random Forest combines the outputs of multiple decision trees to obtain a single result. We used the randomForest package (version 4.7) (Liaw and Weiner, 2002). Random forest algorithms have three primary hyper-parameters that must be set before training. These include node size, number of trees, and number of features sampled. In our scenario, we used the default values proposed by the randomForest function, that is, 500, 17, and 5, for the number of trees, number of features, and node size, respectively.

We used a ten-fold cross-validation with ten realisations; thus, 100 models were constructed. We calculated confusion matrices to calculate the accuracy of the HFST classes. Following the studies of Rossiter (2004) and Salley et al. (2018), we calculated the accuracy as follows:

- Overall accuracy (OA) represents the absolute percentage of HFST classes that match the predicted HFST classes.
- User accuracy (UA) assesses the proportion of HFST classes that match a given predicted HTST class relative to the total number of estimated points of that HFST class (error of commission).
- Producer's reliability (PR) is a measure of the proportion of correctly predicted HFST classes classified by the producer relative to the total

number of observed points within each HFST class (error of omission).

These three indices were calculated as follows:

$$OA = \frac{\sum_{i=1}^{r} E_{ii}}{N} \quad (1)$$

$$UA = \frac{X_{ii}}{\sum_{i=1}^{r} X_{ij}} \quad (2)$$

$$PR = \frac{X_{jj}}{\sum_{i=1}^{r} X_{ij}} \quad (3)$$

where r is the number of texture classes, $E_{ii}$ is the sum of the diagonal elements, N is the number of observations, $X_{ii}$ is the diagonal value for

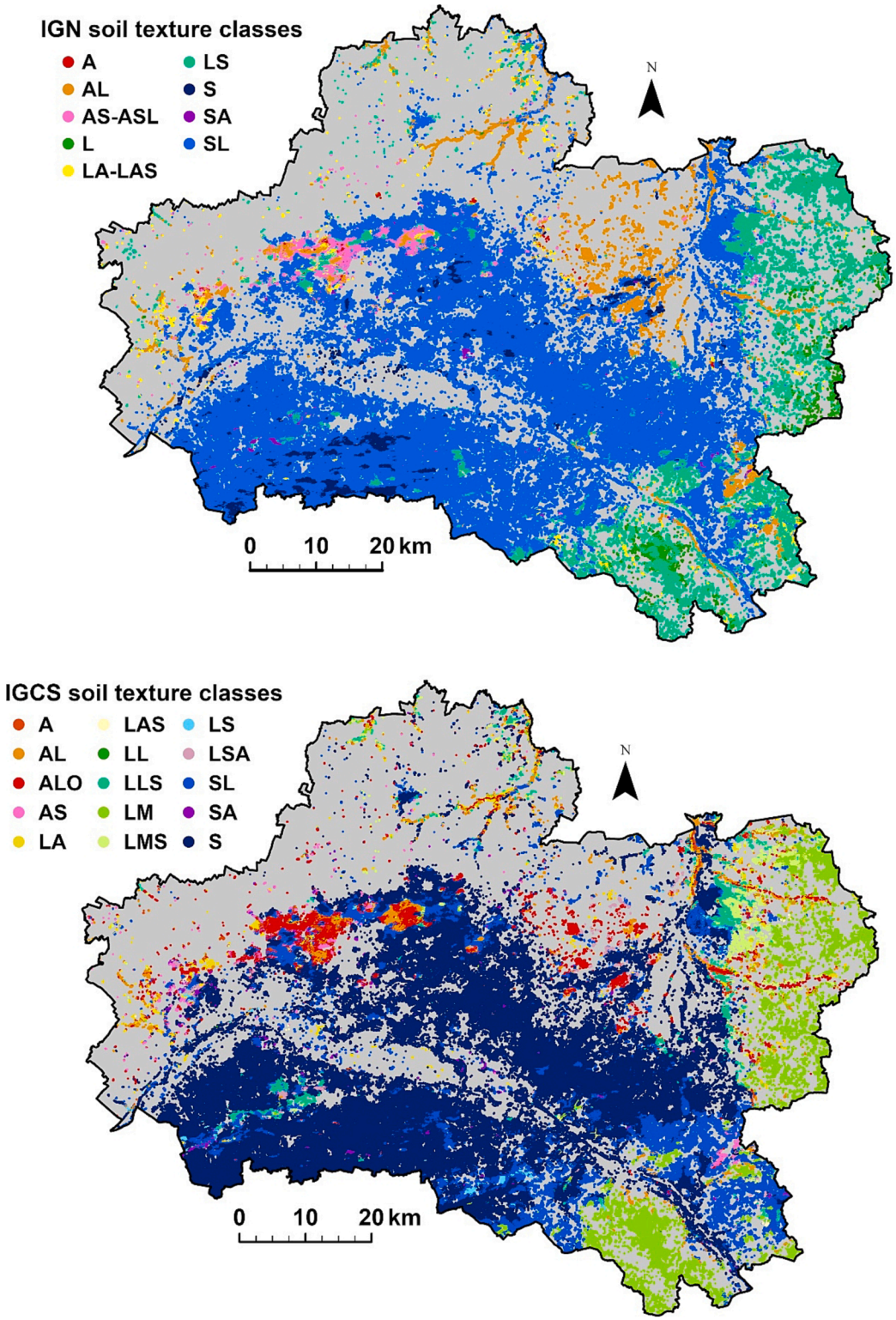


**Fig. 4.** Dominant topsoil textures using the IGN and IGCS observations and triangles.

each class in a row, $X_{ij}$ is the sum of the values in a row or column, and $X_{jj}$ is the diagonal value for each class in a column. Theoretically, OA%, PR %, and UA% can range from 0 % to 100 %, with the most accurate value being 100 %.

These confusion matrices were not derived from an independent probability sampling design. They were based on a ten k-fold validation of the HFST classes. The effects and limitations of this method are discussed in Section 4.2.2.

For mapping, 100 ST classes per pixel were obtained, and we mapped 1) the dominant ST on each pixel and 2) the percentage of predictions of this dominant ST on each pixel as an indicator of prediction consistency.

## 3. Results

### 3.1. Topsoil texture maps

Fig. 4 shows the dominant topsoil textures using the IGN and IGCS observations and triangles.

In general, the maps exhibit similar patterns. The locations of the clayey areas were similar, although a larger variability in the HFST was observed when using the IGCS data than when using the IGN data. This is logical because the clayey IGCS classes are more numerous than the IGN classes. Differences were observed in most clayey areas. The IGCS map exhibits numerous but small areas of heavy clay that were mapped as sandy or loamy clays using the IGN map (Fig. 3). Certain differences in the extreme south-east may also be attributable to sampling density. In the north-east, the spatial patterns were similar, although the differences in texture prediction may have resulted from close but different or intersecting classes in the two triangles (Fig. 2). However, note the differences in the predictions for the valley areas.

Two noticeable differences were observed when observing the large soilscapes dominated by S (IGCS) or SL (IGN):

- Large areas were predicted as SL in the IGN map and as S in the IGCS map. These large areas were primarily located in the Orléans Forest and in Sologne.
- In Sologne, several S patches were revealed by the IGN map but not by the IGCS map.

Therefore, we focused our study on the evaluation of performance and possible explanations for the two differences between the two maps.

Tables 2 and 3 list the results of the cross-validation for the HFST predicted and observed by the IGCS- and IGN-based models.

Both confusion matrices exhibited a low prediction accuracy. For the IGCS (Table 2), the optimal results were obtained for the S class, with an exceedingly high UA% (94.6) and acceptable PR% (67.2), followed by LM (UA% = 74.2; PR% = 60.0). None of the other classes performed well, and certain classes produced poor results. The results for the IGN (Table 3) were misleading, except for the SL class, with a UA% of 88.2. Although the number of classes was higher for the IGCS than for the IGN, its OA% was higher than that for the IGN. However, this result is counter-intuitive. The UA% was excellent for both S-IGCS and SL-IGN, indicating that the model predictions were consistent with their respective input observations in most areas of the Orléans and Sologne Forests. The shortcomings of these matrices are discussed in Section 4.2.2.

### 3.2. Covariate importance

Fig. 5 displays the importance of the covariates estimated by RF for the models using the IGN or IGCS training data.

The four most important covariates were determined using airborne gamma-ray spectrometry. Five of the six most important covariates were obtained from the gamma-ray maps. The most important factor was the K/Th ratio in both models, and the five gamma-ray covariates cited above were the same despite their slight differing orders. Elevation and slope focal means on windows ranging from 100 m to 1 km in radius were among the most important covariates. Certain focal standard deviations of the DEM derivatives were also among the important covariates but to a lesser extent.

### 3.3. Consistencies of the 100 model predictions

Fig. 6 shows the consistency of both predictions, defined as the percentage of the most frequently predicted topsoil texture class among the 100 predictions.

The two maps exhibited similar patterns and value ranges, except for the eastern and extreme northern parts of the département, where the ICGS map appeared slightly less consistent than the IGN map. This effect is partly because the IGN ST classes are larger than those of the IGCS, particularly in the textural domain predicted in these areas (Figs. 2 and 4). This may also be partly due to differences in sampling densities. Overall, the internal consistency of the maps was exceptional, with approximately 89 % and 92 % of the area being consistently predicted (>0.80) and approximately 74 % and 79 % of the prediction area being nearly 'pure' (>0.90), in the IGCS and IGN maps, respectively.

**Table 2**
Confusion matrix between the HFST classes predicted by the model using IGCS HFST as input data and the locally observed IGCS HFST (cross-validation).

| IGCS | | ST class predicted | | | | | | | | | | | | | | | Sum | *UA %* |
|---|---|---|---|---|---|---|---|---|---|---|---|---|---|---|---|---|---|---|
| | **A** | **AL** | **ALO** | **AS** | **LA** | **LAS** | **LL** | **LLS** | **LM** | **LMS** | **LS** | **LSA** | **S** | **SA** | **SL** | | | |
| **ST hand-feel class** | **A** | **2** | 2 | 9 | 0 | 3 | 0 | 0 | 4 | 0 | 2 | 0 | 0 | 10 | 1 | 3 | **36** | ***5.6*** |
| | **AL** | 1 | **12** | 15 | 0 | 5 | 1 | 0 | 0 | 9 | 0 | 1 | 3 | 10 | 0 | 4 | **61** | ***19.7*** |
| | **ALO** | 1 | 8 | **45** | 4 | 3 | 1 | 0 | 1 | 3 | 0 | 0 | 0 | 19 | 1 | 8 | **94** | ***47.9*** |
| | **AS** | 1 | 2 | 9 | **5** | 2 | 0 | 0 | 0 | 0 | 0 | 0 | 1 | 27 | 1 | 6 | **54** | ***9.3*** |
| | **LA** | 0 | 1 | 7 | 2 | **12** | 0 | 0 | 2 | 14 | 5 | 2 | 3 | 5 | 0 | 6 | **59** | ***20.3*** |
| | **LAS** | 0 | 2 | 4 | 0 | 0 | **0** | 0 | 2 | 4 | 0 | 0 | 1 | 12 | 2 | 4 | **31** | ***0.0*** |
| | **LL** | 0 | 0 | 1 | 0 | 0 | 0 | **0** | 0 | 1 | 0 | 0 | 0 | 1 | 0 | 0 | **3** | ***0.0*** |
| | **LLS** | 0 | 1 | 2 | 1 | 0 | 1 | 0 | **12** | 3 | 5 | 1 | 0 | 37 | 0 | 14 | **77** | ***15.6*** |
| | **LM** | 0 | 2 | 4 | 0 | 1 | 0 | 0 | 0 | **72** | 8 | 1 | 1 | 4 | 0 | 4 | **97** | ***74.2*** |
| | **LMS** | 0 | 0 | 1 | 0 | 3 | 0 | 0 | 7 | 8 | **11** | 1 | 0 | 5 | 0 | 4 | **40** | ***27.5*** |
| | **LS** | 1 | 1 | 2 | 2 | 2 | 0 | 0 | 1 | 2 | 0 | **5** | 1 | 14 | 0 | 16 | **47** | ***10.6*** |
| | **LSA** | 1 | 2 | 5 | 1 | 2 | 0 | 0 | 1 | 1 | 1 | 1 | **8** | 23 | 2 | 8 | **56** | ***14.3*** |
| | **S** | 1 | 2 | 2 | 1 | 0 | 0 | 0 | 0 | 2 | 0 | 1 | 1 | **849** | 8 | 30 | **897** | ***94.6*** |
| | **SA** | 0 | 1 | 2 | 1 | 2 | 1 | 0 | 0 | 0 | 0 | 1 | 3 | 83 | **3** | 13 | **110** | ***2.7*** |
| | **SL** | 1 | 3 | 3 | 4 | 1 | 0 | 0 | 6 | 1 | 0 | 3 | 4 | 165 | 1 | **54** | **246** | ***22.0*** |
| **Sum** | **9** | **39** | **111** | **21** | **36** | **4** | **0** | **36** | **120** | **32** | **17** | **26** | **1264** | **19** | **174** | **1908** | | |
| ***PR %*** | ***22.2*** | ***30.8*** | ***40.5*** | ***23.8*** | ***33.3*** | ***0.0*** | ***0.0*** | ***33.3*** | ***60.0*** | ***34.4*** | ***29.4*** | ***30.8*** | ***67.2*** | ***15.8*** | ***31.0*** | | ***OA%= 57.1*** | |

**Table 3**
Confusion matrix between the HFST classes predicted by the model using the IGN HFST as input data and the locally observed IGN HFST (cross-validation).

| IGN | | ST class predicted | | | | | | | | | Sum | *UA%* |
|---|---|---|---|---|---|---|---|---|---|---|---|---|
| | **A** | **AL** | **AS** | **L** | **LA-LAS** | **LS** | **S** | **SA** | **SL** | | | |
| **ST hand-feel class** | **A** | **0** | 9 | 4 | 0 | 1 | 4 | 1 | 0 | 6 | **25** | ***0.0*** |
| | **AL** | 1 | **27** | 8 | 0 | 6 | 27 | 2 | 2 | 54 | **127** | ***21.3*** |
| | **AS** | 2 | 11 | **12** | 1 | 5 | 7 | 2 | 0 | 58 | **98** | ***12.2*** |
| | **L** | 0 | 1 | 1 | **6** | 0 | 40 | 0 | 0 | 6 | **54** | ***11.1*** |
| | **LA-LAS** | 0 | 10 | 8 | 2 | **4** | 32 | 1 | 0 | 70 | **127** | ***3.1*** |
| | **LS** | 0 | 6 | 7 | 11 | 2 | **118** | 1 | 2 | 138 | **285** | ***41.4*** |
| | **S** | 1 | 0 | 0 | 0 | 1 | 3 | **50** | 0 | 180 | **235** | ***21.3*** |
| | **SA** | 0 | 3 | 3 | 0 | 4 | 13 | 2 | **0** | 145 | **170** | ***0.0*** |
| | **SL** | 0 | 7 | 8 | 0 | 9 | 45 | 31 | 2 | **765** | **867** | ***88.2*** |
| **sum** | **4** | **74** | **51** | **20** | **32** | **289** | **90** | **6** | **1422** | **1988** | | |
| ***PR %*** | ***0.0*** | ***36.5*** | ***23.5*** | ***30.0*** | ***12.5*** | ***40.8*** | ***55.6*** | ***0.0*** | ***53.8*** | | ***OA% = 49.4*** | |

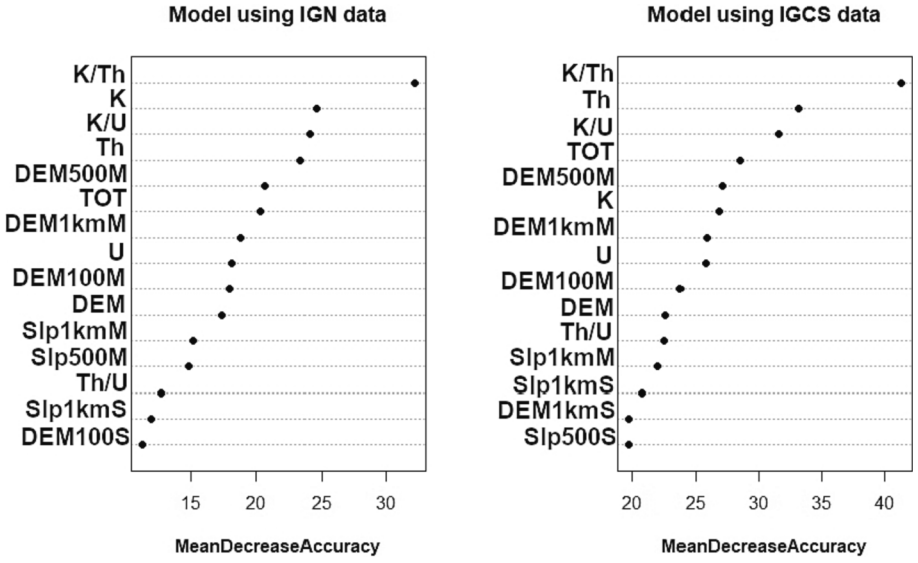


**Fig. 5.** Covariates' importance for the models using the IGN (left) or IGCS data (right).

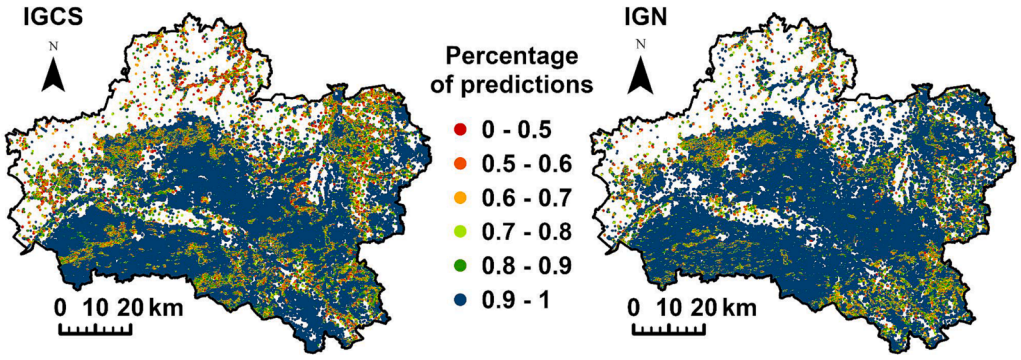


**Fig. 6.** Percentage of predictions among the 100 models of the dominant topsoil texture for the two maps. Left: IGCS, right: IGN.

Nonetheless, these maps convey a markedly distinct message regarding 'consistency' than Tables 2 and 3 do. We investigated whether the 'dominant' ST class in each pixel was consistently predicted, which was the case. However, when comparing the dominant ST values with the values in Tables 2 and 3, the 'dominant' ST class often represents a small percentage. A striking example is the HFST AS predicted by the IGN-based model, which is dominant but with a UA% and PR% of 12.2 % and 23.5 %, respectively. Note that to achieve a deeper analysis of the confusions between repeated predictions, we could have used confusion indices taking into account more classes than the dominant one (Burrough et al., 1997) or entropy indices such as the Shannon's 'H' index (Shannon, 1948; Shannon and Weaver, 1998).

Whatever, these figures and numbers (either those presented in this article, or those who could have been produced using the above mentioned indices) cannot be considered independent accuracy estimates. They provide an estimate of the consistency of predictions among the 100 models. Alternatively stated, they provide an indicator of the repeatability of the predictions of the 100 models. However, they do not provide information on whether these predictions were accurate. They neither determine which map is correct, considering the large S and SL areas, which are predicted differently by the two models, nor the small patches of sand predicted in the southern part using the IGN data. To

estimate the accuracy of the predictions, we required independent validation, as presented in the following sections. In these sections, we focus on S and SL, representing exceedingly large areas of the IGCS and IGN maps. Therefore, we designed independent evaluation schemes as following.

### 3.4. Sampling design and measurements for the local assessment of DSM performances, particle-size analysis, and particle binocular observations

The maps identified two major differences between the predictions (Fig. 4).

Certain large areas were predicted as a sand (S) using the IGCS triangle observations, whereas they were predicted as a sandy loam (SL) using IGN observations. This difference was observed for both Orléans Forest (north of the Loire River) and Sologne Forest (south of the département).

Specific patterns of S textures were observed in Sologne using the IGN data, whereas they were not detected when using the IGCS data. These S patterns were discovered as inclusions within large areas where DSM using the IGN data predicted SL values, whereas most of the Sologne area was predicted as S using the IGCS data.

Therefore, we used two complementary evaluation strategies for these two areas.

#### 3.4.1. Sampling design

1) South of Sologne, we selected a validation area (Fig. 1) and applied stratified design-based probability sampling. Random locations of new sampling points were selected within and outside the S areas mapped using the IGN learning dataset. The number of points was proportional to the areas predicted as S or SL using the IGN model. This resulted in 13 auger borings descriptions and 35 topsoil samples in the S and SL areas, respectively, as predicted by the IGN model. All topsoil horizons were analysed. In total, 48 topsoil samples were transferred to the laboratory and subsequently observed with a binocular microscope.
2) In the Orléans Forest, we selected closely situated points (<75 m apart) with an initially observed topsoil HFST classified as S by the IGCS and SL by the IGN. As in Sologne, all topsoil horizons were sampled and analysed. Because the likelihood of having closely situated points was low, this sampling strategy resulted in only 12 pairs of points.

In total, 72 topsoil samples were analysed in the laboratory, including 24 samples from the Orléans Forest and 48 samples from the Sologne validation area.

For both validation sampling schemes, topsoil was defined as the 0-to-30 cm depth layer (once the O horizons were removed). It corresponded nearly always to A horizons or to the upper part of A horizons. We retained the 0–30 layer when the HFST was homogeneous. In case a change in HFST occurred before 30 cm, we kept the upper part for HFST and/or laboratory analysis. This abrupt change occurred for a small proportion of observations and was always deeper than 20 cm. Therefore, the thickness of the layers retained for analysis ranged from 20 to 30 cm, most of them being equal to 30 cm.

#### 3.4.2. Laboratory soil analyses

The samples were air-dried at a constant temperature and hygrometry (30 °C, 30 % air hygrometry) until a constant weight was achieved.

Particle-size fractionation was performed in eight fractions and coarse fragments (after the removal of soil organic matter by $H_2O_2$ pretreatment). The following fractions were retained: clay (<2 μm), fine silt (2–20 μm), coarse silt (20–50 μm), very fine sand (50–100 μm), fine sand (100–200 μm), three fractions of coarse sand (200–500 μm), (500–1000 μm), (1000–2000 μm), and coarse fragments (>2000 μm). The coarse fragments were measured using the NF ISO 11464 method. Particle-size fractionation was performed using the pipette method (NFX 31-107). The clay, silt, and sand percentages were used to calculate the laboratory-measured ST (LAST).

#### 3.4.3. Microscopy observations

The samples were first treated with $H_2O_2$ to remove organic compounds (Juvigné, 1982; Petigara et al., 2002; Vafaei Molamahmood et al., 2021). The samples were then heated to accelerate the reaction. When the effervescence of the reaction was no longer visible, the samples were washed, sieved at 50 μm to recover the sands and gravels, and then dried at 30 °C.

Binocular analyses were performed at BRGM facilities using a Leica DFC 425 binocular microscope. The morphologies of the sand and coarser particles were observed, and photographs were captured. When feasible, the minerals were identified.

#### 3.4.4. Consistency of soilscape locations in the Sologne area

The locations of the S areas predicted using the IGN data were compared with their locations relative to the primary small river network. We created transects projecting the topography and gamma-ray emissions along the line segments intersecting the small valleys and IGN model areas with different predicted STs (S or SL), and we interpolated the gamma-ray emissions.

### 3.5. Results of the local independent evaluations

#### 3.5.1. HFST and particle-size analysis

In this section, we attempt to estimate whether a systematic bias exists between the S and SL predictions when using the IGCS or IGN HFST data.

*3.5.1.1. HFST and particle-size analysis in the Orléans forest.* Fig. 7 shows the results of laboratory analysis of soil texture (LAST) measurements on pairs of closely situated points classified as S or SL by HFST during the initial sampling campaigns of the IGCS and IGN in the Orléans Forest.

Among the twelve points predicted as SL by the IGN-HFST observations, ten were identified as S when performing the LAST measurements. This implies that the SL IGN-HFST estimates were biased toward approximately 83 % of the observations. Conversely, nine of twelve points predicted as S by the IGCS-HFST observations were consistent with the LAST measurements, indicating that IGCS-HFST correctly predicted the S texture for approximately 75 % of the observations. Although the total number of points sampled was low, these results suggest a systematic bias exists in the IGN surveyor observations. This bias is not linked to the effect of the difference between the limits of the S and SL classes in the two triangles.

*3.5.1.2. Predicted HFST and particle-size analysis in the Sologne evaluation area.* In this section, we use a stratified random probability sampling design to evaluate whether the S and SL textures are correctly predicted in the Sologne evaluation area. Fig. 8 shows the LAST results obtained for the topsoil samples located in the spatial patterns predicted as S using the IGN model.

These predictions led to the observation of spatial patterns not present in the IGCS map (Fig. 4).

- The projected LAST of the topsoil samples belonging to the IGN-predicted S patterns (blue) showed that 12 of 13 samples effectively corresponded to the LAST measurements when projected on the IGN triangle. Using the IGCS triangle, this correspondence was observed in 11 of the 13 samples. This result suggests that the patterns revealed by the IGN-based model can be considered nearly pure sand areas.
- Conversely, considering the samples outside the S areas predicted by the IGN model, which were predicted as S by the IGCS model (blue)

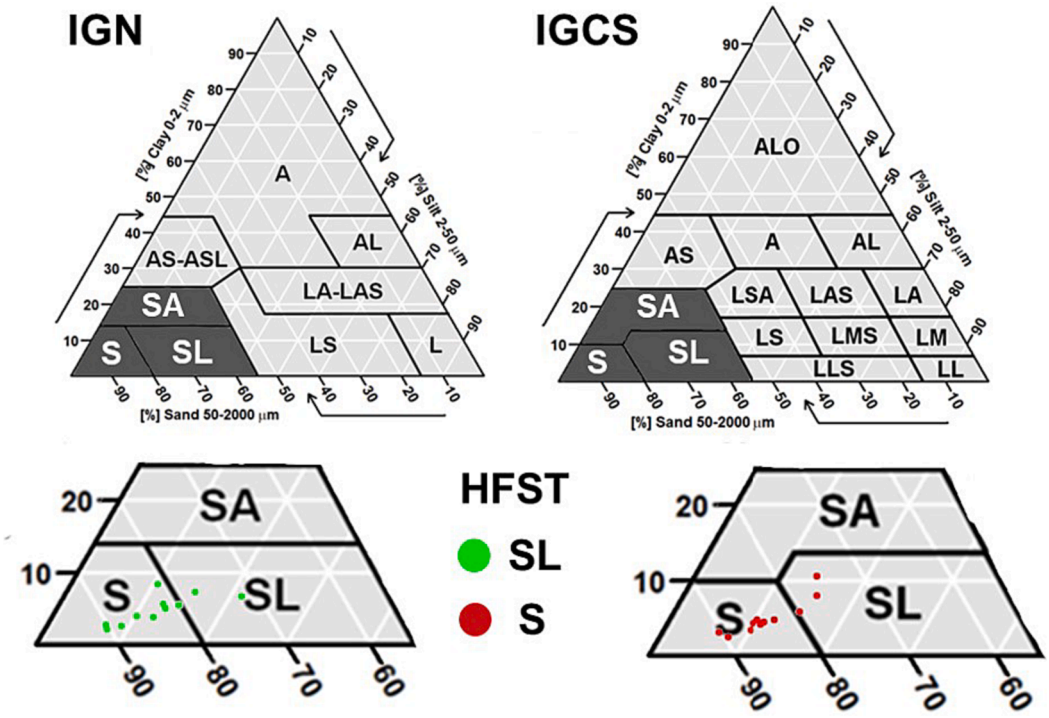


**Fig. 7.** Projection in both the IGCS (right) and IGN (left) triangles of the results of the laboratory analysis (LAST) performed on closely situated pairs of topsoil layers classified in situ by HFST during the initial surveys as S (red) or SL (green) by the IGCS and IGN respectively.

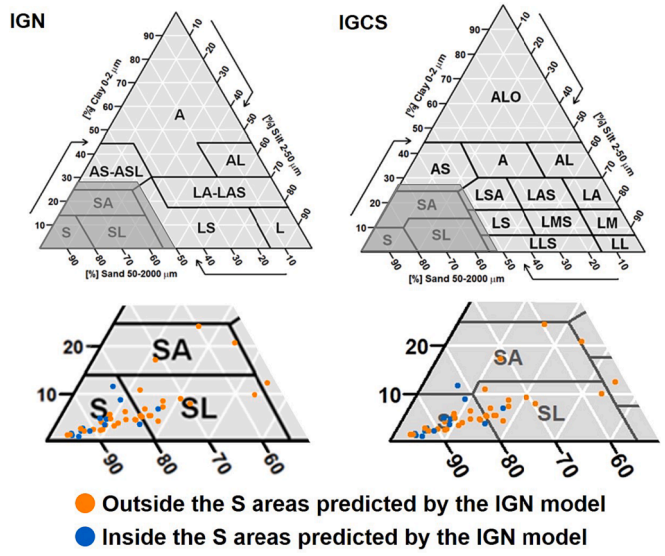


**Fig. 8.** LAST topsoil textures as projected on the IGN (left) and IGCS (right) soil texture triangles. Blue: samples located inside the areas predicted as S by the IGN model. Orange: samples located outside the areas predicted as S by the IGN model, as SL by the IGN model, and as S by the IGCS model.

and as SL by the IGN model (orange): in this area, thirteen of thirty-five samples were effectively SL, eighteen were S, and four were other textural classes adjacent to S + SL. Therefore, in this area, we observed S and SL in 51 % and 37 % of the cases, respectively. Independent sampling showed that this area is characterised by an association of S and SL, representing approximately 88 % of the observed points, with the remainder of the other points belonging to textures adjacent to S + SL. In addition, within this area, S dominated the SL.

- Our results query why the IGN observations and model could reveal nearly pure sand patterns. Outside these patterns, they query if it is logical to attempt mapping 'pure' ST classes or if certain areas should be better characterised by an association of S and SL ST classes and their relative proportions.

Fig. 9 displays the box plots of sand with coarse fragment content in percentage (i.e. equivalent to g.100 $g^{-1}$) inside (A) and outside (B) the areas predicted as sand by the IGN model.

The box plots are distinctly different. The sand and coarse element contents were substantially higher inside the areas predicted as S by the IGN model than those outside. These results suggest that the processes and/or nature of the deposits were different in areas A and B.

*3.5.2. Gamma-ray signature statistical distributions inside and outside the areas predicted as S by the IGN model*

Fig. 10 shows the statistical distribution of the airborne gamma-ray spectrometry interpolated emissions inside (yellow) and outside (dark

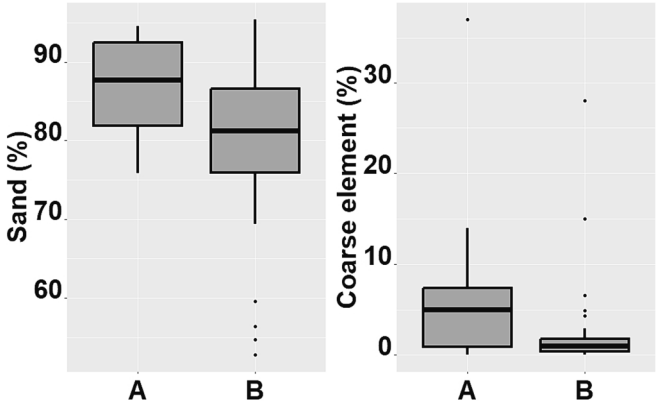


**Fig. 9.** Box plots of topsoil sand and coarse element content (% = g.100 $g^{-1}$). (A) Inside and (B) outside the areas predicted as sand by the IGN model.

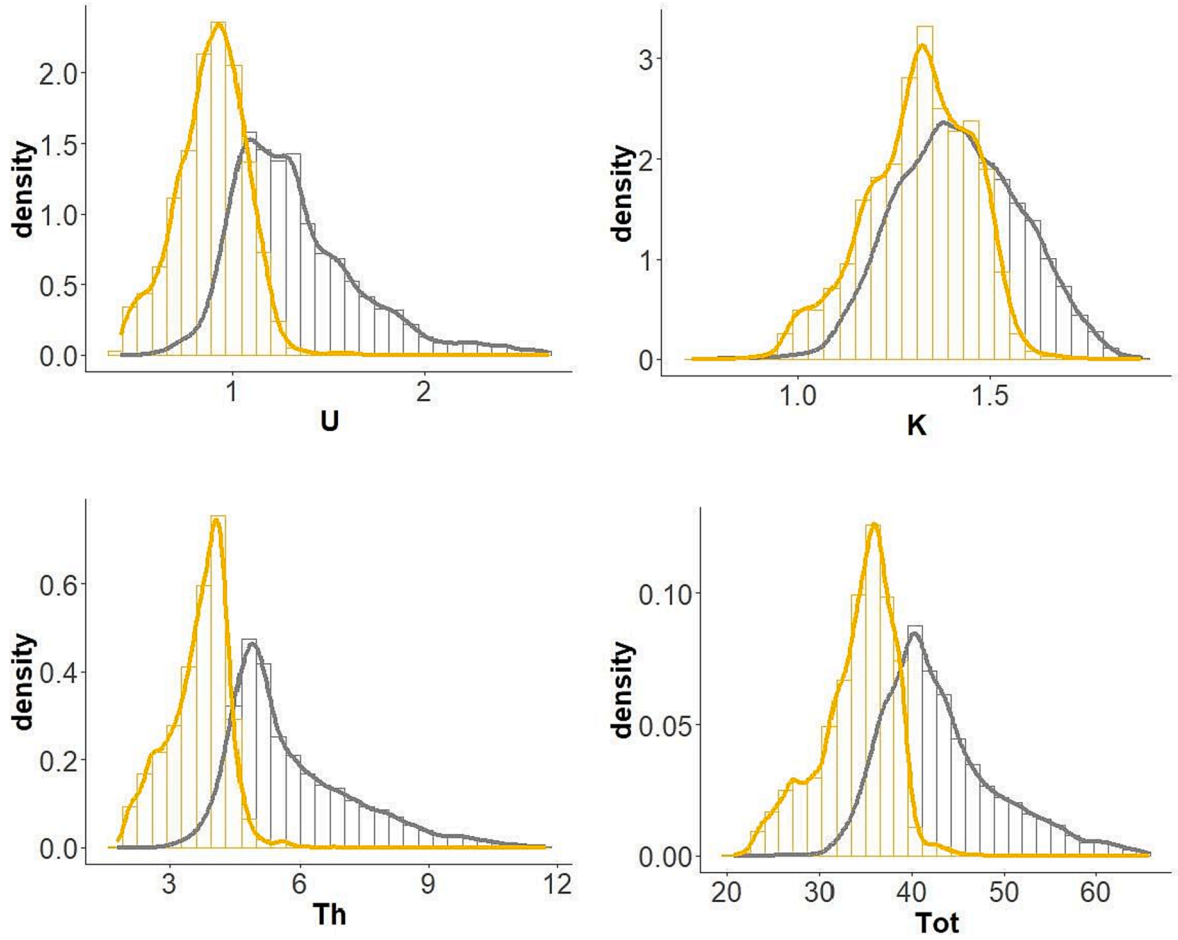


**Fig. 10.** Histograms and fitted statistical distributions of airborne gamma-ray spectrometric values of U, K, Th, and total count (Tot) inside (yellow) and outside (dark grey) the areas predicted as S by the IGN model.

grey) the areas predicted as S by the IGN model.

The distributions inside the areas predicted as S showed more distinct and sharper peaks and lower modal values of gamma-ray emissions than those observed outside these areas. We observed an overlap between the distributions, which was largely dependent on the origin of the emissions. Note the sharp decrease on the right side of the distribution of areas predicted as S. This decrease indicates that high emission values were scarcely observed in the areas predicted to be S by the IGN model. These distributions were smoothed by interpolation, and resampling was used to allocate gamma-ray emissions to each pixel. Considering the smoothing effect, the results obtained are noteworthy and suggest that the actual difference in emissions from these two populations may be further differentiated.

### 3.5.3. Microscopy observations

Fig. 11 shows four examples of microscope observations of samples predicted as S (left column A) or SL (right column B) using the IGN model. The organic matter was removed using $H_2O_2$.

Microscope observations confirmed that particles coarser than (or approximately) 2 mm were more numerous in areas predicted as S than in those predicted as SL. We interpret these results as an amplified 'gritty' tactile sensation when certain particles are coarser than others. This effect likely led the IGN surveyors to distinguish A areas with S HFST from B areas considered less sandy than these areas and thus classified as SL HFST. As the observations were performed in forests, it cannot be excluded that some SL HFST could have been influenced by the presence of organic matter, which may have provided a soft tactile sensation similar to that of silt. Nearly all the sand samples were pure silica quartz. In area B, other minerals were occasionally observed (e.g. feldspars) but in few cases and especially low proportions (data not shown). The images cannot be used to estimate the relative proportions of coarse elements (>2 mm) for at least two reasons: 1) the coarser particles mask some underlying finer particles, and 2) the sand and gravel are not precisely spherical, which is a recurrent scenario influencing the 2 mm sieving results.

### 3.5.4. Consistency with geomorphology and landscape position

Fig. 12 shows the locations of the S patterns revealed by the IGN model.

The majority of these patterns were located along the three primary small rivers flowing from east to west. These patterns follow the primary direction of the rivers, and their shapes are generally elongated in the direction of the river current. These observations suggest the presence of terraces created by alluvial deposits originating from the east and transported by these small rivers when they were significantly larger than presently. This hypothesis is consistent with the findings of Tissoux et al. (2017), who identified alluvial deposits along these small rivers. However, their maps were substantially less detailed than those in this study, which is understandable because they studied a substantially larger area than we did, using the same gamma-ray data, but with an objective and sampling design markedly distinct from ours. Nonetheless, the results of Tissoux et al. (2017) are consistent with those of the present study.

Fig. 13 shows an example of a transect from points A to B based on Fig. 12.

Fig. 13 shows that the three areas predicted as pure S are located

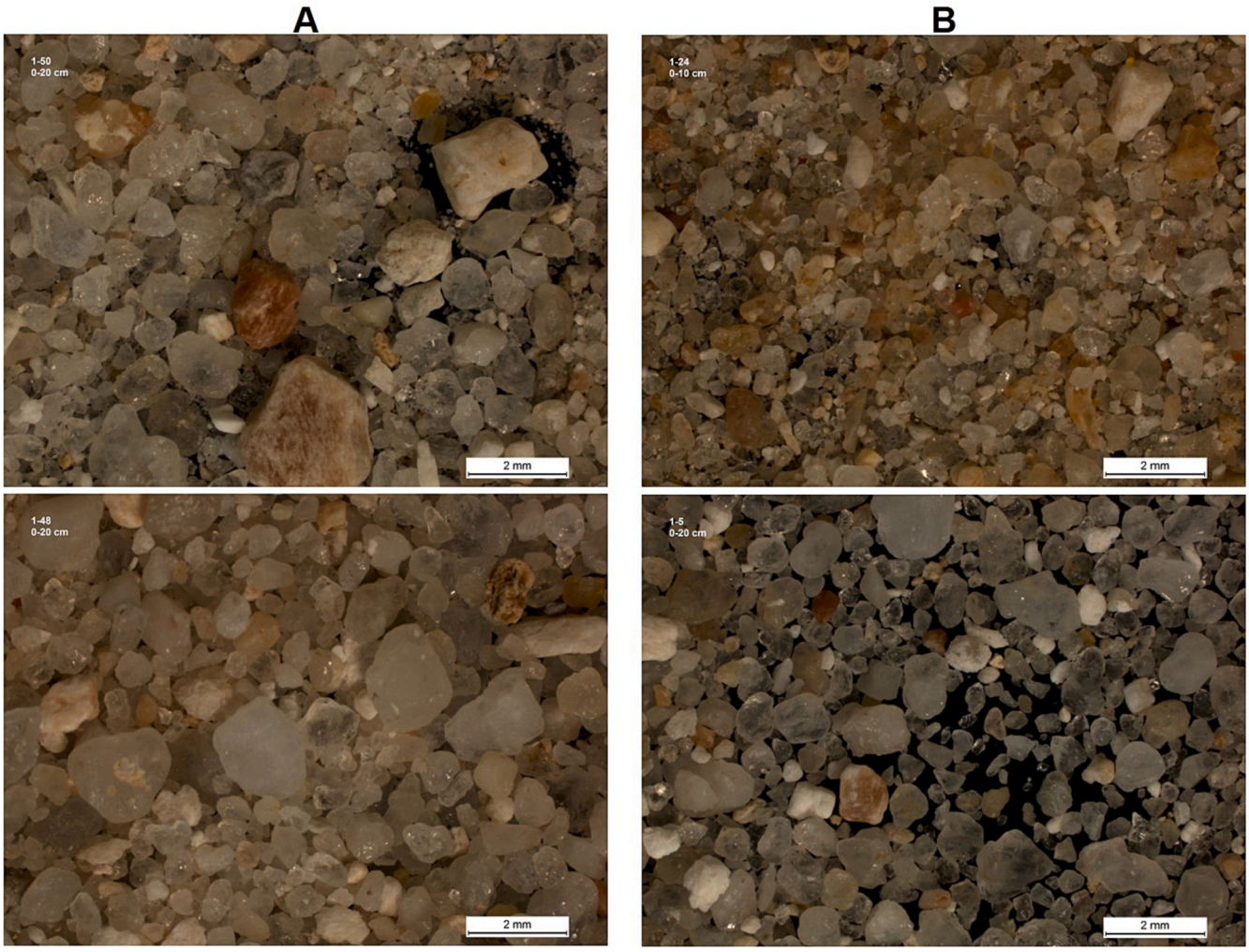


**Fig. 11.** Selection of certain binocular observation images. (A) Inside and (B) outside the areas predicted as S by the IGN model.

within similar elevation ranges (120–130 m). These areas exhibited the lowest Th emissions and are located in flat regions. These observations are consistent with the alluvial origin of these S areas, which originates from materials that may have been transported from farther eastern locations. The specificity of these pure S materials was corroborated by their pure sand LAST values and the presence of particles coarser than 2 mm.

Another low Th emission, but in a substantially higher elevation area than that in the other areas, was identified in this transect. This area corresponds to the ancient terrace of the Loire River but has a different origin. This terrace is gravelly and has highly weathered and illuviated sandy soils (Horemans, 1962). Therefore, its gamma-ray signature is logical. The RF IGN model results primarily depend on both gamma-ray emissions and relief attributes (Fig. 5). Therefore, the prediction of pure S areas likely excluded this terrace because of its DEM-derived attributes. This observation corroborates the importance of the DEM attributes smoothed over large windows.

## 4. Discussion

### *4.1. Principal findings—comparison with other studies*

#### *4.1.1. Utility of HFST data*

The topsoil HFST point observations were beneficial for predicting ST patterns using the DSM, as we observed consistent patterns of contrasted HFST for both ST triangles and inventory programmes. These findings suggest that the HFST can be inexpensive and useful information to incorporate as an input variable in the DSM of ST. HFST determinations are substantially less precise than those of LAST but can be substantially more numerous. HFST can be relatively reliable depending on the operators and triangles used (e.g. Carlile et al., 2001; Franzmeier and Owens, 2008; Richer-de-Forges et al., 2022; Vos et al., 2016).

In contrast, certain systematic biases between the two sampling campaigns and triangles confirm that HFST determination can be subjective and that its accuracy may depend on the experience of the soil surveyors and the range of particle-size fractions present over a study area (Foss et al., 1975; Levine et al., 1989; Salley et al., 2018).

In the present study, the two evaluation sampling initiatives (in the northern and southern parts) distinctly showed a systematic bias in the IGN HFST input data. In the northern part, we showed that for S and SL, the IGCS HFST observations by soil surveyors were more accurate than the IGN observations. The IGN HFST observations underestimated the S class and overestimated the SL class. Therefore, from a textural class perspective, the input data used to map the S and SL classes should be more efficient when using the IGCS framework. One hypothesis is that soil surveyors of the ICGS framework were more experienced than those in the IGN framework and have benefited from the cross-checks of the HFST and LAST for a prolonged period in various landscapes.

Nonetheless, this bias in the IGN input data was crucial in identifying the nearly pure silica sandy and relatively gravelly terraces in southern Sologne. This ‘biased’ observations, in conjunction with relevant covariates (particularly airborne gamma-ray data), proved highly efficient

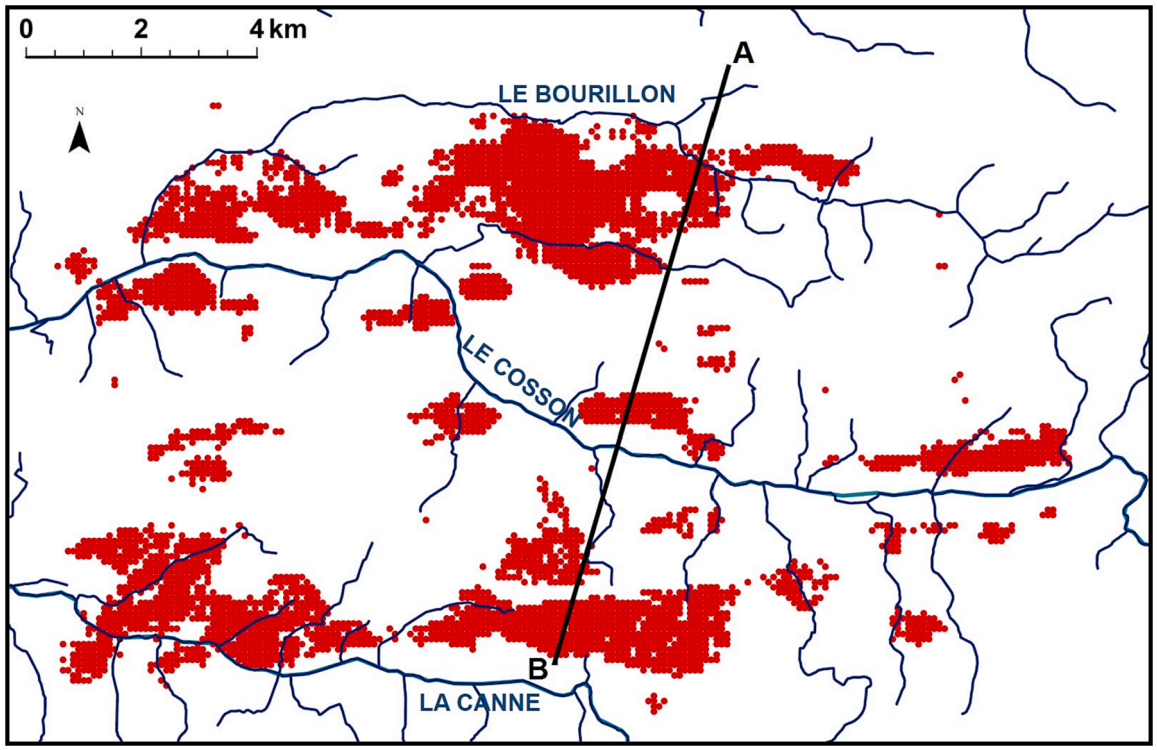


**Fig. 12.** Location of areas identified as S by the IGN model (red) and of the primary small rivers flowing from east to west in the Sologne validation area. The (A–B) line segment corresponds to the transect shown in Fig. 13.

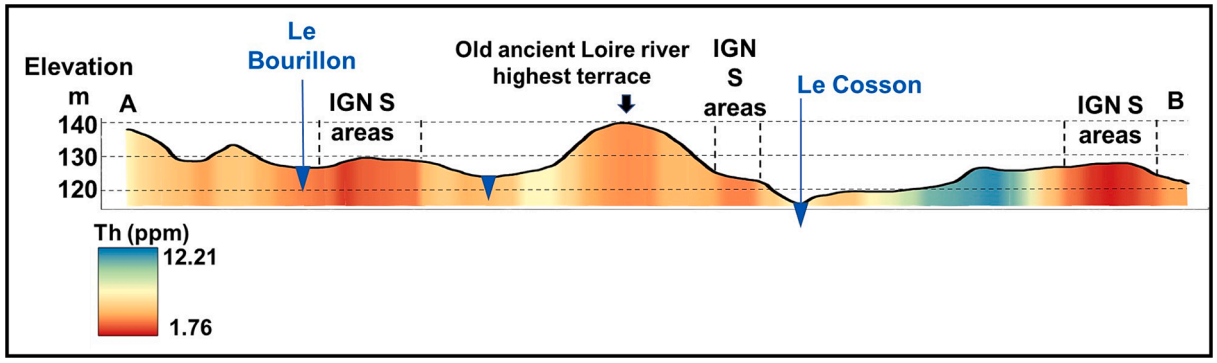


**Fig. 13.** Transect from points A to B (Fig. 12) showing the elevation, gradients of gamma-ray spectrometry Th emission, and the locations of the two primary rivers flowing from east to west. The unnamed river is a small tributary of 'Le Cosson', the source of which is located in the validation area and not from an eastern location distant from this area.

for capturing certain patterns that were not identified using the IGCS input data. This result shows that, regardless of the biased observations, they provided useful information on soil spatial distribution. These results suggest that discarding data on the sole criteria of accuracy may lead to missing 'hidden' information that is provided by the spatial distribution and/or clustering of certain field observations.

*4.1.2. Utility of gamma-ray spectrometry*

For both models (with the IGCS or IGN HFST input data), raw gamma-ray spectrometry data and ratios were the most important covariates for predicting the topsoil HFST. This aligns with numerous studies that have mapped topsoil texture in various regions and landscapes worldwide [e.g. Taylor et al. (2002) in Australia, Rawlins et al. (2007) in England, Van Der Klooster et al. (2011) in The Netherlands, Priori et al. (2014, 2013) in Italy, Heggemann et al. (2017) in Germany, and Martelet et al. (2013) and Loiseau et al. (2020) in France]. Soil gamma-ray emissions are highly correlated with clay content and mineralogy (e.g. Reinhardt and Herrmann, 2019; Wilford, 2002; Wilford and Minty, 2006). Thus, our case study is a noteworthy example owing to the high variability in clay content (from heavy clay to nearly pure quartz sand). Moreover, we showed that gamma-ray spectrometry can detect different natures of sand, size distributions, and sand contents within the sand texture class. These results are exceptional and exceed our expectations.

Although the signal of gamma-ray emissions is attenuated by forest cover, it can capture information from the topsoil layers. The exact contribution of the topsoil thickness to emissions is unknown. However, some studies have suggested that, in mineral soils, the contribution to emissions strongly decreases with depth (Reinhardt and Herrmann, 2019) and that approximately 90 % of the emissions may originate from the upper 20–25 cm of mineral soil (Grasty, 1997). This depth is consistent with the thicknesses of the sampled topsoil horizons, ranging from 20 to 45 cm.

The quality of these results is likely enhanced owing to the forested

study area not including the following: (i) high emissions linked to some sesquioxides, such as those observed in some tropical areas (Bednar et al., 2004; Taylor et al., 2002); ii) natural mineralisation outcrops of high-emitting elements (else they would have been detected on the gamma-ray maps); (iii) high levels of soil contamination in emitting elements (which would have also been detected); and (iv) the perturbing effects of agricultural management and fertilization on gamma-ray emissions (e.g. Wetterlind et al., 2012b, 2012a).

#### 4.1.3. Utility of relief attributes

For both models, relief attributes contributed to the prediction of the HFST. Notably, we observed the utility of raw DEM values and their derivatives at different scales of spatial aggregation. The benefit of using various scales for relief attribute covariates aligns with that of previous studies (e.g. Behrens et al., 2010; Chen et al., 2021; Grinand et al., 2008; Loiseau et al., 2020, 2019; Sena et al., 2020).

The most noteworthy result was the consistency between the exceedingly low gamma-ray emissions, pure silica sand, and the geomorphology in the southern part of the Sologne Forest. This consistency is exceptional and should be emphasised. The relief attributes also contributed to avoiding confusion between the Loire River's high terrace and the small Sologne Rivers terraces, regardless of whether they might be similar from an ST or gamma-ray perspective.

As several studies have suggested (e.g. Arrouays et al., 2020a; Wadoux et al., 2020b, 2020a; Wadoux and McBratney, 2021), the goodness of DSM predictions should not be evaluated using statistical estimators alone. Other criteria should examine whether the predictions and choice of covariates are logical from a soil science and landscape perspective. In this study, we showed that DSM may help highlight certain processes (in the present study, specific alluvial deposits) that are confirmed by ST, mineralogy, sand morphology and content, coarse elements, gamma-ray emissions, landform, and position in the landscape.

#### 4.1.4. Potential additional pathway to improve DSM performance

Several case studies have compared several models, sampling strategies, or sets of covariates to demonstrate the optimal selection for predicting a given soil attribute using DSM (see a review from Chen et al., 2022). They have often based their conclusions on optimal prediction performance indicators. Unfortunately, most of these conclusions are case-specific. Other studies have used an equivalent comparison to determine whether the results were consistent among different approaches. This strategy may be useful for testing whether certain changes in the datasets (e.g. increasing the density of points and adding new covariates) have similar and generic effects, regardless of the models. Finally, certain studies have proposed averaging or mixing several predictions using ensemble modelling, leading to the logical hypothesis that ensemble modelling is more robust than using only one model.

In the present study, we tested two soil attribute inputs. Using a range of prediction performance indicators on an overall independent dataset of ST across the entire map would likely have led to the conclusion that the IGCS dataset was optimal. However, we did not attempt to select the optimal dataset for the entire map. We explored whether there was any useful information for each dataset. Having completed this action, we showed that a dataset that would have been rejected using the overall estimates of prediction performance could be useful for specific soilscapes.

#### 4.1.5. Mapping larger ST classes may be logical

The results obtained for the probability sampling evaluation areas are consistent. They showed that certain large areas identified as S by the IGCS model and SL by the IGN model were, in actuality, characterised by an ensemble of ST composed of approximately 50 % S, 40 % SL, and 10 % other ST classes adjacent to this ensemble. From scientific and practical perspectives, stating that these areas are S with an accuracy of 50 % is substantially less informative than mapping an ensemble and defining this ensemble by an S + SL association with an accuracy of 90 % and internal relative proportions of S and SL of approximately 56 % and 44 %, respectively. Alternatively stated, we should recognise that there are cases where DSM was not efficient for mapping 'pure' ST. This may be due to the local variability of S and SL that could not be captured using our learning data density and covariates. However, DSM could map certain ensembles that were logical and could be characterised by their relative proportions. In contrast, the S areas revealed by only the IGN model were nearly pure S with some gravel, and mapping them as pure sand ST units appeared feasible and logical.

To formulate this conclusion, independent probability sampling was necessary and proved to be highly efficient. We lacked the financial means to conduct probability sampling across the entirety of the département, which is a limitation of the present study.

### 4.2. Limitations of the study

#### 4.2.1. Data availability

This study used input variables and covariates, the availability of which may depend strongly on their locations.

The input soil information (HFST) for learning is inexpensive and easily gathered. However, the density of point data may vary significantly among and even within countries (Arrouays et al., 2017b). Several countries do not yet possess soil maps at a scale of 1:250,000 and related databases with geolocalised soil observations. Inventories based on a systematic 1 $km^2$ cell grid, such as that conducted by IGN for forest soils in mainland France, are rarer than these soil maps and related databases. Even in France, such a fine grid does not exist for land covers other than forests. We may consider the feasibility of implementing such a density of information and sampling design worldwide. Considering cost and access constraints, the response was that it was not feasible.

The covariates used for the DSM may also have different spatial coverages and precisions (Richer-de-Forges et al., 2023a, 2023b; Samuel-Rosa et al., 2015). If we can logically state that precise DEMs are currently available worldwide owing to remote sensing, this is in stark contrast to the reality of airborne gamma-ray spectrometry. There are relatively few countries with full airborne gamma-ray spectrometry coverage. Evidently, most airborne gamma-ray surveys have been inspired by mining objectives (primarily for uranium; IAEA, 2010, 1976), and their acquisition over large areas represents a significant financial cost. Therefore, obtaining airborne gamma-ray spectrometry data from soils worldwide in the next decade is unlikely. For example, the coverage of mainland France using this covariate is currently approximately 40 %. Nonetheless, previous studies in similar contexts have demonstrated the high potential of airborne gamma-ray spectrometry for topsoil texture mapping. In addition, the coverage of gamma-ray data is gradually but continuously increasing in France and several countries worldwide. Airborne gamma-ray spectrometry also had some limitations in the present study because of the smoothing effect linked to interpolations. Proximal gamma-ray spectrometry can be a useful tool for obtaining geographically precise information and/or estimating the effect of interpolation on the precision of airborne gamma-ray covariates.

#### 4.2.2. Necessity for validation and mapping uncertainties

The confusion matrices shown in Tables 2 and 3 cannot be considered independent validation results for the département. They were not constructed using independent probability sampling. They were derived from the k-fold validation of the initial dataset. Therefore, they only indicate whether the predictions are consistent with the observations. Therefore, they likely overestimate the goodness of prediction and do not consider possible errors linked to biases in HFST estimation. Distances between classes, or between LAST measurements and HFST classes (see for example Richer-de-Forges et al. (2023a)), could have

been incorporated into the model evaluation in order to lessen the effect of near misses as opposed to huge misses in mis-classification. An independent probability sampling design combined with LAST measurements was conducted for a specific area of interest. However, conducting such probability sampling over the entirety of the département was not feasible in the framework of this study.

Because of high costs, few DSM studies can gather independent data for validation purposes. Over relatively large areas, the method used for estimating prediction performance is primarily cross-validation (Chen et al., 2022). An independent, stratified random sampling design is often limited to small areas. For example, one option proposed by Malone et al. (2011) is to select a limited number of strata, hypothesising that if the ensemble of covariates can be clustered into different groups, then these groups should have similar internal variability and prediction intervals. Another option, more similar to the option we retained, would be to select a set of sub-areas representing different physiographies and soilscapes and concentrate the independent validation effort on these sub-areas.

In the present study, we primarily focused our validation efforts on the S and SL ST. This strategy was consistent with the observation that these STs covered the majority of the area and that we observed systematic differences between the two HFST datasets. We also aimed to determine if the unexpected sandy spatial structures observed in southern Sologne using IGN HFST existed and whether their locations and characteristics had plausible explanations and specific properties and origins. We neither explored nor validated the predictions for the other texture classes.

### 4.3. Perspectives

#### 4.3.1. Improving ST predictions at the département level

In this study, the LAST results were not incorporated into the soil profiles obtained during the IGCS soil survey. Combining precise analytical values with more uncertain data, such as the HFST, is feasible, although by no means trivial (e.g. Malone and Searle, 2021a, 2021b). In the future, we plan to verify this approach.

We could also attempt to disaggregate the 1:250,000 soilscape map, as proposed by Odgers et al. (2014a,2014b) and applied with various adaptations in several studies (e.g. Chaney et al., 2016; Easher et al., 2023; Ellili-Bargaoui et al., 2020a, 2020b, 2019; Holmes et al., 2015; Jamshidi et al., 2019; Møller et al., 2019; Vincent et al., 2018). Finally, these approaches could be combined to obtain the optimal predictions.

Regardless of the approach, it would require a more exhaustive independent validation test on the entire département.

#### 4.3.2. Enlarging the study to mainland France

Several DSM predictions of ST or clay, silt, sand, and/or coarse element contents have already been produced at the scale of mainland France (Caubet et al., 2019; Mulder et al., 2016a; Román Dobarco et al., 2019). The first map (Mulder et al., 2016a) uses available LAST data from the IGCS programme (latest date, 2014) and approximately 2,200 LAST site measurements from the French soil monitoring network based on a 16 × 16 km systematic grid. The second map (Caubet et al., 2019) merges several ST predictions at different scales (national, EU, and global). The third map (Román Dobarco et al., 2019) uses the IGCS data for calibration and RMQS data for validation.

None of these maps used the HFST estimates. In addition, the IGCS programme has an unbalanced sampling density between forest and agricultural areas. Because of the history of soil mapping in France, sampling points under forest were substantially less dense than those in agricultural landscapes.

Considering the disparity in the sampling densities and designs of the aforementioned datasets, the availability of a systematic 1 km HFST grid for all forested land (approximately 31 % of mainland France, i.e. 17.1 million ha) could constitute an excellent opportunity to improve ST prediction over the entire mainland France. As the first IGN campaign already covered all forested areas and is currently undergoing a subsequent iteration, there are currently approximately 190,000 IGN sites in the database. The use of all these IGN HFST data at national level would require further work to estimate the consistency between HFST and LAST over the French territory and to assess the benefit of adding rather uncertain data (HFST). Further studies should deal with the trade-off between adding noise in the measurements and filling the geographical space when using HFST.

Other data sources of topsoil LAST are increasing in quantity, such as those collected in the framework of the French Soil Test Database (BDAT; e.g. Lemercier et al., 2008; Saby et al., 2017), which gathers soil analyses realised under the requests of farmers, and for which an increasing quantity of locations are now geolocalised. However, these analyses are conducted only on agricultural soil and there are still some legal limitations about the use of their precise geolocalisation in France.

## 5. Conclusions

The primary conclusions of this pilot study at the French département scale are as follows:

- HFST data provided useful information as a learning variable in DSM.
- Two different HFST datasets with different ST triangles and relatively experienced surveyors provided slightly different results, even when using the same covariates. However, most patterns in the topsoil ST maps were consistent.
- Using two different sampling designs, we underlined a systematic bias in one dataset.
- Even if biased, the HFST dataset remains useful for detecting specific soilscapes. Therefore, before discarding certain learning data based on a possible bias, we recommend testing and verifying whether using this dataset helps capture specific patterns or spatial structures.
- Depending on the scale, density of observations, and covariates, predicting associations characterised by their relative percentage in two STs may be more relevant than attempting to predict a given ST alone. However, predicting nearly pure ST was possible in specific and contrasting cases.
- The DEM derivatives and gamma-ray data helped detect specific patterns. They contributed to revealing and explaining patterns that were logical from both soil process and soil management perspectives.
- We should not consider certain data as unusable because they do not satisfy certain statistical criteria. We must also examine the map produced and attempt to explain the unexpected findings, if any.
- Numerous HFST datasets exist and should not be ignored. We should continue to recover these data and explore their potential for improving DSM and soil process knowledge at a low cost.

**Data availability**

The 1/250,000 soilscape map of the Loiret and its associated book (both in paper format) are sold by QUAE editions (France). https://www.quae.com/collection/13/cartes-et-referentiels-pedologiques.

Points coordinates and associated soil data in private properties are not publicly available, according to French regulations.

The Loiret 1/250,000 soilscape map in digital format and its related database are available for free upon reasonable request and license agreement. The database is described in Richer-de-Forges et al. (2008), and the link to the database is available at https://doi.org/10.15454/1U255W. People willing to have free access to data should precise the framework and the intended utilization of the map. All products using this map should cite and acknowledge its source. The database does not include points data, but areal statistics and estimates of soil types and soil properties mean, minimum and maximum values. Neither INRAE, nor the author are responsible for misuses of the data, nor for possible errors and/or uncertainties in the map and the related

database.

The IGN forest soils grid is the property of the National Institute for Geographic and Forest Information. The access to point data is restricted and requests should be made through the "Information Forestières" website: https://inventaire-forestier.ign.fr/.

The IGN DEM at 25 m resolution (BD ALTI ®) is the property of the National Institute for Geographic and Forest Information (IGN). All départment data are downloadable at: https://geoservices.ign.fr/bdalti/.

Airborne gamma-ray data used in this study are available from BRGM upon request.

## CRediT authorship contribution statement

**Alexandre Eymard:** . **Anne C. Richer-de-Forges:** . **Guillaume Martelet:** Investigation, Methodology, Resources, Writing – original draft, Writing – review & editing. **Hélène Tissoux:** . **Anne Bialkowski:** Conceptualization, Data curation, Formal analysis, Funding acquisition, Investigation, Methodology, Project administration, Resources, Supervision, Validation, Writing – original draft, Writing – review & editing. **Marine Dalmasso:** Investigation, Methodology, Project administration, Resources, Validation, Writing – original draft, Writing – review & editing. **Fabrice Chrétien:** Validation, Writing – original draft, Writing – review & editing. **David Belletier:** Validation, Writing – original draft, Writing – review & editing. **Guillaume Ledemé:** Investigation, Methodology, Resources, Writing – original draft, Writing – review & editing. **Didier Laloua:** Validation, Writing – original draft, Writing – review & editing. **Olivier Josière:** Methodology, Writing – original draft, Writing – review & editing. **Loïc Commagnac:** . **Hocine Bourennane:** Conceptualization, Methodology, Supervision, Validation, Writing – original draft, Writing – review & editing. **Dominique Arrouays:** Conceptualization, Formal analysis, Funding acquisition, Investigation, Methodology, Resources, Supervision, Validation, Writing – original draft, Writing – review & editing.

## Declaration of competing interest

The authors declare that they have no known competing financial interests or personal relationships that could have appeared to influence the work reported in this paper.

## Acknowledgements

The airborne gamma-spectrometric data used in this study were financed by Région Centre, BRGM, France, and FEDER European funds. The sampling and most of the soil analyses were funded by a French Scientific Group of Interest on Soils, the "GIS Sol", involving the French Ministry for Ecology and Sustainable Development, the French Ministry of Agriculture, the French Agency for Energy and Environment (ADEME), the French National Research Institute for Agriculture, Food and Environment (INRAE), the French Institute for Research and Development (IRD, France), the National Forest Inventory (IGN), The French Biodiversity Agency (OFB), and by local département, region, and Agricultural Chamber funds.

We thank L. Bailly for providing access to BRGM DGR-GEM binocular facilities. We thank all of the soil surveyors and technical assistants involved in sampling the sites, preparing soils samples, and producing soil analyses. This research was conducted within the "Centre d'Expertise Scientifique Cartographie Numérique des Sols" granted by the CNES TOSCA program. The work of Alexandre Eymard was granted by the French Ministry in charge of agriculture, INRAE and IGN. We thank Jingyi Huang and Budiman Minasny for their helpful comments and discussions on this work. We thank the two anonymous reviewers for their helpful and constructive comments on a previously submitted version of this paper and for their proposals that helped to improve it.

## References

Arrouays, D., Grundy, M.G., Hartemink, A., Hempel, J., Heuvelink, G., Hong, S., Lagacherie, P., Lelyk, G., McBratney, A., McKenzie, N., Mendonca-Santos, M., Minasny, B., Montanarella, L., Odeh, I., Sanchez, P., Thompson, J., Zhang, G., 2014a. GlobalSoilMap: Toward a Fine-Resolution Global Grid of Soil Properties, in: Sparks, D. (Ed.), Advances in Agronomy. p. 93. https://doi.org/10.1016/B978-0-12-800137-0.00003-0.

Arrouays, D., McBratney, A.B., Minasny, B., Hempel, J.W., Heuvelink, G.B.M., MacMillan, R.A., Hartemink, A.E., Lagacherie, P., McKenzie, N.J., 2014. The GlobalSoilMap specifications. In: GlobalSoilMap. Basis of the Global Spatial Soil Information System. Taylor and Francis, London, United Kingdom, pp. 9–12.

Arrouays, D., Lagacherie, P., Hartemink, A.E., 2017a. Digital soil mapping across the globe. Geoderma Reg. 9, 1–4. https://doi.org/10.1016/j.geodrs.2017.03.002.

Arrouays, D., Leenaars, J.G.B., Richer-de-Forges, A.C., Adhikari, K., Ballabio, C., Greve, M., Grundy, M., Guerrero, E., Hempel, J., Hengl, T., Heuvelink, G., Batjes, N., Carvalho, E., Hartemink, A., Hewitt, A., Hong, S.-Y., Krasilnikov, P., Lagacherie, P., Lelyk, G., Libohova, Z., Lilly, A., McBratney, A., McKenzie, N., Vasquez, G.M., Mulder, V.L., Minasny, B., Montanarella, L., Odeh, I., Padarian, J., Poggio, L., Roudier, P., Saby, N., Savin, I., Searle, R., Solbovoy, V., Thompson, J., Smith, S., Sulaeman, Y., Vintila, R., Rossel, R.V., Wilson, P., Zhang, G.-L., Swerts, M., Oorts, K., Karklins, A., Feng, L., Ibelles Navarro, A.R., Levin, A., Laktionova, T., Dell'Acqua, M., Suvannang, N., Ruam, W., Prasad, J., Patil, N., Husnjak, S., Pásztor, L., Okx, J., Hallett, S., Keay, C., Farewell, T., Lilja, H., Juilleret, J., Marx, S., Takata, Y., Kazuyuki, Y., Mansuy, N., Panagos, P., Van Liedekerke, M., Skalsky, R., Sobocka, J., Kobza, J., Eftekhari, K., Alavipanah, S.K., Moussadek, R., Badraoui, M., Da Silva, M., Paterson, G., da Gonçalves, M. da C., Theocharopoulos, S., Yemefack, M., Tedou, S., Vrscaj, B., Grob, U., Kozák, J., Boruvka, L., Dobos, E., Taboada, M., Moretti, L., Rodriguez, D., 2017b. Soil legacy data rescue via GlobalSoilMap and other international and national initiatives. GeoResJ 14, 1–19. https://doi.org/10.1016/j.grj.2017.06.001.

Arrouays, D., McBratney, A., Bouma, J., Libohova, Z., Richer-de-Forges, A.C., Morgan, C. L.S., Roudier, P., Poggio, L., Mulder, V.L., 2020a. Impressions of digital soil maps: The good, the not so good, and making them ever better. Geoderma Reg. 20, e00255.

Arrouays, D., Poggio, L., Salazar Guerrero, O.A., Mulder, V.L., 2020b. Digital soil mapping and GlobalSoilMap. Main Advances and Ways Forward. Geoderma Reg. 21, e00265.

Batschelet, E., 1981. Circular statistics in biology, Mathematics in biology. Academic Press, London.

Bednar, A.J., Gent, D.B., Gilmore, J.R., Sturgis, T.C., Larson, S.L., 2004. Mechanisms of Thorium Migration in a Semiarid Soil. J. Environ. Qual. 33, 2070–2077. https://doi.org/10.2134/jeq2004.2070.

Behrens, T., Zhu, A.-X., Schmidt, K., Scholten, T., 2010. Multi-scale digital terrain analysis and feature selection for digital soil mapping. Geoderma 155, 175–185. https://doi.org/10.1016/j.geoderma.2009.07.010.

Bourennane, H., King, D., Couturier, A., 2000. Comparison of kriging with external drift and simple linear regression for predicting soil horizon thickness with different sample densities. Geoderma 97, 255–271. https://doi.org/10.1016/S0016-7061(00)00042-2.

Breiman, L., 2001. Random forests. Mach. Learn. 45, 5–32. https://doi.org/10.1023/A:1010933404324.

Burrough, P.A., van Gaans, P.F.M., Hootsmans, R., 1997. Continuous classification in soil survey: spatial correlation, confusion and boundaries. Geoderma 77, 115–135. https://doi.org/10.1016/S0016-7061(97)00018-9.

Carlile, P., Bui, E., Moran, C., Minasny, B., McBratney, A.B., 2001. Estimating soil particle size distributions and percent sand, silt and clay for six texture classes using the Australian Soil Resource Information System point database (Technical Report 29/01). CSIRO Land and Water, Canberra.

Caubet, M., Román Dobarco, M., Arrouays, D., Minasny, B., Saby, N.P.A., 2019. Merging country, continental and global predictions of soil texture: Lessons from ensemble modelling in France. Geoderma 337, 99–110. https://doi.org/10.1016/j.geoderma.2018.09.007.

Chaney, N.W., Wood, E.F., McBratney, A.B., Hempel, J.W., Nauman, T.W., Brungard, C. W., Odgers, N.P., 2016. POLARIS: A 30-meter probabilistic soil series map of the contiguous United States. Geoderma 274, 54–67. https://doi.org/10.1016/j.geoderma.2016.03.025.

Chartin, C., Stevens, A., Goidts, E., Krüger, I., Carnol, M., Van Wesemael, B., 2017. Mapping Soil Organic Carbon stocks and estimating uncertainties at the regional scale following a legacy sampling strategy (Southern Belgium, Wallonia). Geoderma Reg. 9, 73–86. https://doi.org/10.1016/j.geodrs.2016.12.006.

Chen, S., Richer-de-Forges, A.C., Leatitia Mulder, V., Martelet, G., Loiseau, T., Lehmann, S., Arrouays, D., 2021. Digital mapping of the soil thickness of loess deposits over a calcareous bedrock in central France. Catena 198, 105062. https://doi.org/10.1016/j.catena.2020.105062.

Chen, S., Arrouays, D., Leatitia Mulder, V., Poggio, L., Minasny, B., Roudier, P., Libohova, Z., Lagacherie, P., Shi, Z., Hannam, J., Meersmans, J., Richer-de-Forges, A. C., Walter, C., 2022. Digital mapping of GlobalSoilMap soil properties at a broad scale: A review. Geoderma 409, 115567. https://doi.org/10.1016/j.geoderma.2021.115567.

Cluzeau, C., Drapier, J., 2001. La base de données écologiques de l'IFN. Une approche factorielle et synthétique des écosystèmes forestiers. Les 40 ans de l'IFN - Utilisation et valorisation des données collectées. Revue Forestière Française LIII, 391–396 [in French].

Easher, T.H., Saurette, D., Chappell, E., Lopez, F.D.J.M., Gasser, M.-O., Gillespie, A., Heck, R.J., Heung, B., Biswas, A., 2023. Sampling and classifier modification to

DSMART for disaggregating soil polygon maps. Geoderma 431, 116360. https://doi.org/10.1016/j.geoderma.2023.116360.
Ellili-Bargaoui, Y., Walter, C., Michot, D., Saby, N.P.A., Vincent, S., Lemercier, B., 2019. Validation of digital maps derived from spatial disaggregation of legacy soil maps. Geoderma 356, 113907. https://doi.org/10.1016/j.geoderma.2019.113907.
Ellili-Bargaoui, Y., Malone, B.P., Michot, D., Minasny, B., Vincent, S., Walter, C., Lemercier, B., 2020a. Comparing three approaches of spatial disaggregation of legacy soil maps based on the Disaggregation and Harmonisation of Soil Map Units Through Resampled Classification Trees (DSMART) algorithm. Soil 6, 371–388. https://doi.org/10.5194/soil-6-371-2020.
Ellili-Bargaoui, Y., Walter, C., Michot, D., Lemercier, B., 2020b. Mapping soil properties at multiple depths from disaggregated legacy soil maps in the Brittany region, France. Geoderma Reg. 23, e00342.
Foss, J.E., Wright, W.R., Coles, R.H., 1975. Testing the Accuracy of Field Textures. Soil Sci. Soc. Am. J. 39, 800–802. https://doi.org/10.2136/sssaj1975.03615995003900040051x.
Franzmeier, D.P., Owens, P.R., 2008. Soil Texture Estimates: A Tool to Compare Texture-by-Feel and Lab Data. J. Nat. Resour. Life Sci. Educ. 37, 111–116.
Giot, D., 2002. Carte géologique du Loiret à 1/125 000. Bureau de Recherches Géologiques et Minières, Paris [in French].
Grasty, R., 1997. Radon emanation and soil moisture effects on airborne gamma-ray measurements. Geophysics 62, 1379–1385. https://doi.org/10.1190/1.1444242.
Grinand, C., Arrouays, D., Laroche, B., Martin, M.P., 2008. Extrapolating regional soil landscapes from an existing soil map: Sampling intensity, validation procedures, and integration of spatial context. Geoderma 143, 180–190. https://doi.org/10.1016/j.geoderma.2007.11.004.
Heggemann, T., Welp, G., Amelung, W., Angst, G., Franz, S.O., Koszinski, S., Schmidt, K., Pätzold, S., 2017. Proximal gamma-ray spectrometry for site-independent in situ prediction of soil texture on ten heterogeneous fields in Germany using support vector machines. Soil Tillage Res. 168, 99–109. https://doi.org/10.1016/j.still.2016.10.008.
Heung, B., Ho, H.C., Zhang, J., Knudby, A., Bulmer, C.E., Schmidt, M.G., 2016. An overview and comparison of machine-learning techniques for classification purposes in digital soil mapping. Geoderma 265, 62–77. https://doi.org/10.1016/j.geoderma.2015.11.014.
Holmes, K.W., Griffin, E.A., Odgers, N.P., 2015. Large-area spatial disaggregation of a mosaic of conventional soil maps: evaluation over Western Australia. Soil Res. 53, 865. https://doi.org/10.1071/SR14270.
Horemans, P., 1962. Contribution à l'étude pédologique des terrasses alluviales de la Loire moyenne. (Thèse de doctorat). Faculté des Sciences de l'Université de Paris, Paris. [in French].
IAEA, 1976. Exploration of uranium ore deposits., in: Proceedings of Symposium. Presented at the International atomic energy agency (IAEA) and OECD nuclear energy agency, International atomic energy agency (IAEA) and OECD nuclear energy agency, Vienna, Austria, p. 867.
IAEA, 1991. Airborne gamma ray spectrometer surveying (Technical Reports No. Series No. 323.). IAEA.
IAEA, 2003. Guidelines for radioelement mapping using gamma ray spectrometry data (IAEA-TECDOC-1363.).
IAEA, 2010. Radioelement Mapping (No. IAEA Nuclear Energy Series, N° NF-T-1.3). International Atomic Energy Agency, Vienna.
IGN, 2011. BD ALTI® Version 2.0 - Descriptif de Contenu. [in French].
Jamagne, M., 1967. Bases et techniques d'une cartographie des sols. Annales agronomiques, Numéro hors série [in French].
Jamshidi, M., Delavar, M.A., Taghizadehe-Mehrjardi, R., Brungard, C., 2019. Disaggregation of conventional soil map by generating multi realizations of soil class distribution (case study: Saadat Shahr plain, Iran). Environ. Monit. Assess. 191, 769. https://doi.org/10.1007/s10661-019-7942-x.
Joly, D., Brossard, T., Cardot, H., Cavailhes, J., Hilal, M., Wavresky, P., 2010. Les types de climats en France, une construction spatiale. cybergeo. [in French]. https://doi.org/10.4000/cybergeo.23155.
Juvigné, E., 1982. L'utilisation rationnelle de l'eau oxygénée pour la destruction de matières organiques en granulométrie. Bulletin De La Société Géographique De Liège 19–29 [in French].
Kamamia, A.W., Vogel, C., Mwangi, H.M., Feger, K.-H., Sang, J., Julich, S., 2021. Mapping soil aggregate stability using digital soil mapping: A case study of Ruiru reservoir catchment, Kenya. Geoderma Reg. 24, e00355.
Kidd, D., Searle, R., Grundy, M., McBratney, A., Robinson, N., O'Brien, L., Zund, P., Arrouays, D., Thomas, M., Padarian, J., Jones, E., Bennett, J.M., Minasny, B., Holmes, K., Malone, B.P., Liddicoat, C., Meier, E.A., Stockmann, U., Wilson, P., Wilford, J., Payne, J., Ringrose-Voase, A., Slater, B., Odgers, N., Gray, J., van Gool, D., Andrews, K., Harms, B., Stower, L., Triantafilis, J., 2020. Operationalising digital soil mapping – Lessons from Australia. Geoderma Reg. 23, e00335.
King, D., Bourennane, H., Isambert, M., Macaire, J.J., 1999. Relationship of the presence of a non-calcareous clay–loam horizon to DEM attributes in a gently sloping area. Geoderma 89, 95–111. https://doi.org/10.1016/S0016-7061(98)00124-4.
Lacquement, F., Prognon, F., Tourlière, B., Martelet, G., Deparis, J., Tissoux, H., Reninger, P.-A., Perrin, J., 2015. Méthodologie de cartographie du régolithe à partir de données radiométriques aéroportées en région Centre - Etablissement de cartes lithologiques (Rapport BRGM Orléans No. BRGM/RP-64932-FR). BRGM, Orléans. [in French].
Lemercier, B., Gaudin, L., Walter, C., Aurousseau, P., Arrouays, D., Schvartz, C., Saby, N.P.A., Follain, S., Abrassart, J., 2008. Soil phosphorus monitoring at the regional level by means of a soil test database. Soil Use Manag. 24, 131–138. https://doi.org/10.1111/j.1475-2743.2008.00146.x.
Lemercier, B., Lagacherie, P., Amelin, J., Sauter, J., Pichelin, P., Richer-de-Forges, A.C., Arrouays, D., 2022. Multiscale evaluations of global, national and regional digital soil mapping products in France. Geoderma 425, 116052. https://doi.org/10.1016/j.geoderma.2022.116052.
Levine, S., Post, D.F., Ellsworth, T., 1989. An evaluation of student proficiency in field estimation of soil texture. J. Agronom. Educ. 18, 100–104.
Liard, M., Tissoux, H., Deschamps, S., 2017. Les alluvions anciennes de la Loire en orléanais (France, Loiret), une relecture à l'aune de travaux d'archéologie préventive et d'un programme de datations ESR. Quaternaire 105–128. [in French]. https://doi.org/10.4000/quaternaire.7914.
Liaw, A., Weiner, M., 2002. Classification and Regression by randomForest. R News 2, 18–22. https://CRAN.R-project.org/doc/Rnews/.
Loiseau, T., Chen, S., Mulder, V.L., Román Dobarco, M., Richer-de-Forges, A.C., Lehmann, S., Bourennane, H., Saby, N.P.A., Martin, M.P., Vaudour, E., Gomez, C., Lagacherie, P., Arrouays, D., 2019. Satellite data integration for soil clay content modelling at a national scale. Int. J. Appl. Earth Obs. Geoinf. 82, 101905 https://doi.org/10.1016/j.jag.2019.101905.
Loiseau, T., Richer-de-Forges, A.C., Martelet, G., Bialkowski, A., Nehlig, P., Arrouays, D., 2020. Could airborne gamma-spectrometric data replace lithological maps as covariates for digital soil mapping of topsoil particle-size distribution? A case study in Western France. Geoderma Reg. 22, e00295.
Ma, Y., Minasny, B., Malone, B.P., Mcbratney, A.B., 2019. Pedology and digital soil mapping (DSM). Eur. J. Soil Sci. 70 (2), 216–235. https://doi.org/10.1111/ejss.12790.
Macaire, J.J., 1985. Relations entre les altérites formées sur les roches endogènes du Massif central français et les épandages détritiques périphériques, au Cénozoïque récent. Géol. Fr. 2, 201–212 [in French].
Malone, B., Searle, R., 2021a. Updating the Australian digital soil texture mapping (Part 1*): re-calibration of field soil texture class centroids and description of a field soil texture conversion algorithm 16.
Malone, B., Searle, R., 2021b. Updating the Australian digital soil texture mapping (Part 2*): spatial modelling of merged field and lab measurements 17.
Malone, B.P., McBratney, A.B., Minasny, B., 2011. Empirical estimates of uncertainty for mapping continuous depth functions of soil attributes. Geoderma 160, 614–626. https://doi.org/10.1016/j.geoderma.2010.11.013.
Mardia, K.V., 1972. Statistics of Directional Data. Academic Press, London.
Martelet, G., Drufin, S., Tourliere, B., Saby, N.P.A., Perrin, J., Deparis, J., Prognon, F., Jolivet, C., Ratié, C., Arrouays, D., 2013. Regional Regolith Parameter Prediction Using the Proxy of Airborne Gamma Ray Spectrometry. Vadose Zone J. 12, vzj2013.01.0003 https://doi.org/10.2136/vzj2013.01.0003.
Martelet, G., Nehlig, P., Arrouays, D., Messner, F., Tourlière, B., Laroche, B., Deparis, J., Saby, N.P.A., Richer-de-Forges, A.C., Jolivet, C., Ratié, C., 2014. Airborne gamma-ray spectrometry: potential for regolith-soil mapping and characterization., in: GlobalSoilMap: Basis of the Global Spatial Soil Information System. Taylor & Francis, CRC Press, London, pp. 401–408.
McBratney, A.B., Mendonça Santos, M.L., Minasny, B., 2003. On digital soil mapping. Geoderma 117, 3–52. https://doi.org/10.1016/S0016-7061(03)00223-4.
Minai, J.O., Libohova, Z., Schulze, D.G., 2021. Spatial prediction of soil properties for the Busia area, Kenya using legacy soil data. Geoderma Reg. 25, e00366.
Minasny, B., McBratney, A.B., 2016. Digital soil mapping: A brief history and some lessons. Geoderma 264, 301–311. https://doi.org/10.1016/j.geoderma.2015.07.017.
Minty, B.R.S., 1988. A review of airborne gamma-ray spectrometric data-processing techniques. Bureau of Mineral Resources, Canberra, Australia.
Minty, B., 1997. Fundamentals of airborne gamma-ray spectrometry. AGSO J. Aust. Geol. Geophys. 17, 39–50.
Moeys, J., Shangguan, W., Petzold, R., Minasny, B., Rosca, B., Jelinski, N., Zelazny, W., Marcondes Silva Souza, R., Safanelli, J.L., ten Caten, A., 2018. R package "soiltexture": Functions for Soil Texture Plot, Classification and Transformation.
Møller, A.B., Malone, B., Odgers, N.P., Beucher, A., Iversen, B.V., Greve, M.H., Minasny, B., 2019. Improved disaggregation of conventional soil maps. Geoderma 341, 148–160. https://doi.org/10.1016/j.geoderma.2019.01.038.
Mulder, V.L., Lacoste, M., Richer-de-Forges, A.C., Arrouays, D., 2016a. GlobalSoilMap France: High-resolution spatial modelling the soils of France up to two meter depth. Sci. Total Environ. 573, 1352–1369. https://doi.org/10.1016/j.scitotenv.2016.07.066.
Mulder, V.L., Lacoste, M., Richer-de-Forges, A.C., Martin, M.P., Arrouays, D., 2016b. National versus global modelling the 3D distribution of soil organic carbon in mainland France. Geoderma 263, 16–34. https://doi.org/10.1016/j.geoderma.2015.08.035.
Odgers, N.P., McBratney, A., Minasny, B., Sun, W., Clifford, D., 2014a. Dsmart: An algorithm to spatially disaggregate soil map units. In: Arrouays, D., McKenzie, N., Hempel, J., Richer-de-Forges, A.C., McBratney, A.B. (Eds.), GlobalSoilMap - Basis of the Global Spatial Soil Information System. CRC Press, pp. 261–266. https://doi.org/10.1201/b16500-49.
Odgers, N.P., Sun, W., McBratney, A.B., Minasny, B., Clifford, D., 2014b. Disaggregating and harmonising soil map units through resampled classification trees. Geoderma 214–215, 91–100. https://doi.org/10.1016/j.geoderma.2013.09.024.
Owens, P.R., Dorantes, M.J., Fuentes, B.A., Libohova, Z., Schmidt, A., 2020. Taking digital soil mapping to the field: Lessons learned from the Water Smart Agriculture soil mapping project in Central America. Geoderma Reg. 22, e00285.
Padarian, J., Minasny, B., McBratney, A.B., 2019. Using deep learning for digital soil mapping. Soil 5 (1), 79–89. https://doi.org/10.5194/soil-5-79-2019.
Petigara, B.R., Blough, N.V., Mignerey, A.C., 2002. Mechanisms of Hydrogen Peroxide Decomposition in Soils. Environ. Sci. Tech. 36, 639–645. https://doi.org/10.1021/es001726y.

Poggio, L., de Sousa, L.M., Batjes, N.H., Heuvelink, G.B.M., Kempen, B., Ribeiro, E., Rossiter, D., 2021. SoilGrids 2.0: producing soil information for the globe with quantified spatial uncertainty. Soil 7, 217–240. https://doi.org/10.5194/soil-7-217-2021.

Priori, S., Bianconi, G., Fantapié, M., Pellegrini, S., Ferrigno, G., Guaitoli, F., Costantini, E.A.C., 2013. The potential of γ-ray spectroscopy for soil proximal survey in clayey soils. EQA – Int. J. Environ. Qual. 11 (11), 29–38. https://doi.org/10.6092/ISSN.2281-4485/4086.

Priori, S., Bianconi, N., Costantini, E.A.C., 2014. Can γ-radiometrics predict soil textural data and stoniness in different parent materials? A comparison of two machine-learning methods. Geoderma 226–227, 354–364. https://doi.org/10.1016/j.geoderma.2014.03.012.

Rawlins, B.G., Lark, R.M., Webster, R., 2007. Understanding airborne radiometric survey signals across part of eastern England. Earth Surf. Proc. Land. 32, 1503–1515. https://doi.org/10.1002/esp.1468.

Rawlins, B.G., Scheib, C., Tyler, A.N., Beamish, D., 2012. Optimal mapping of terrestrial gamma dose rates using geological parent material and aerogeophysical survey data. J. Environ. Monit. 14, 3086. https://doi.org/10.1039/c2em30563a.

Reinhardt, N., Herrmann, L., 2019. Gamma-ray spectrometry as versatile tool in soil science: A critical review. J. Plant Nutr. Soil Sci. https://doi.org/10.1002/jpln.201700447.

Richer-de-Forges, A.C., Renaux, B., Verbèque, B., Soucémarianadin, L.N., Eimberck, M., 2008. Référentiel Régional Pédologique de la région Centre : carte des pédopaysages du Loiret à 1/250 000 [In French]. Edition Quae, Paris.

Richer-de-Forges, A.C., Arrouays, D., Chen, S., Román Dobarco, M., Libohova, Z., Roudier, P., Minasny, B., Bourennane, H., 2022. Hand-feel soil texture and particle-size distribution in central France. Relationships and Implications. CATENA 106155. https://doi.org/10.1016/j.catena.2022.106155.

Richer-de-Forges, A.C., Arrouays, D., Poggio, L., Chen, S., Lacoste, M., Minasny, B., 2023a. Hand-feel soil texture observations to evaluate the accuracy of digital soil maps for local prediction of particle size distribution. A case study in central France. Pedosphere 33 (5), 731–743. https://doi.org/10.1016/j.pedsph.2022.07.009.

Richer-de-Forges, A.C., Chen, Q., Baghdadi, N., Chen, S., Gomez, C., Jacquemoud, S., Martelet, G., Mulder, V.L., Urbina-Salazar, D., Vaudour, E., Weiss, M., Wigneron, J.-P., Arrouays, D., 2023b. Remote Sensing Data for Digital Soil Mapping in French Research—A Review. Remote Sens. (Basel) 15, 3070. https://doi.org/10.3390/rs15123070.

Richer-de-Forges, A.C., 2008. Base de données du Référentiel Régional Pédologique de la région Centre : carte des pédopaysages du Loiret à 1/250 000, en format DoneSol2.0. Label de qualité supérieure. [In French]. https://doi.org/10.15454/1U255W.

Román Dobarco, M., Bourennane, H., Arrouays, D., Saby, N.P.A., Cousin, I., Martin, M.P., 2019. Uncertainty assessment of GlobalSoilMap soil available water capacity products: A French case study. Geoderma 344, 14–39.

Rossiter, D.G., 2004. Technical Note: Statistical methods for accuracy assessment of classified thematic maps. Geographical Information Science 1–46. Available online: http://citeseerx.ist.psu.edu/viewdoc/download?doi=10.1.1.77.247&rep=rep1&type=pdf (accessed on 11 August 2023).

Saby, N.P.A., Swiderski, C., Lemercier, B., Walter, C., Louis, B.P., Eveillard, P., Arrouays, D., 2017. Is pH increasing in the noncalcareous topsoils of France under agricultural management? A statistical framework to overcome the limitations of a soil test database. Soil Use Manag. 33, 460–470. https://doi.org/10.1111/sum.12369.

Salley, S.W., Herrick, J.E., Holmes, C.V., Karl, J.W., Levi, M.R., McCord, S.E., van der Waal, C., Van Zee, J.W., 2018. A Comparison of Soil Texture-by-Feel Estimates: Implications for the Citizen Soil Scientist. Soil Sci. Soc. Am. J. 82, 1526–1537. https://doi.org/10.2136/sssaj2018.04.0137.

Samuel-Rosa, A., Heuvelink, G.B.M., Vasques, G.M., Anjos, L.H.C., 2015. Do more detailed environmental covariates deliver more accurate soil maps? Geoderma 243–244, 214–227. https://doi.org/10.1016/j.geoderma.2014.12.017.

Sena, N.C., Veloso, G.V., Fernandes-Filho, E.I., Francelino, M.R., Schaefer, C.E.G.R., 2020. Analysis of terrain attributes in different spatial resolutions for digital soil mapping application in southeastern Brazil. Geoderma Reg. 21, e00268.

Shannon, C.E., 1948. A Mathematical Theory of Communication. Bell Syst. Tech. J. 27, 379–423. https://doi.org/10.1002/j.1538-7305.1948.tb01338.x.

Shannon, C.E., Weaver, W., 1998. The mathematical theory of communication. University of Illinois Press, Urbana.

Taghizadeh-Mehrjardi, R., Minasny, B., Sarmadian, F., Malone, B.P., 2014a. Digital mapping of soil salinity in Ardakan region, central Iran. Geoderma 213, 15–28. https://doi.org/10.1016/j.geoderma.2013.07.020.

Taghizadeh-Mehrjardi, R., Sarmadian, F., Minasny, B., Triantafilis, J., Omid, M., 2014b. Digital Mapping of Soil Classes Using Decision Tree and Auxiliary Data in the Ardakan Region, Iran. Arid Land Res. Manag. 28, 147–168. https://doi.org/10.1080/15324982.2013.828801.

Taghizadeh-Mehrjardi, R., Minasny, B., Toomanian, N., Zeraatpisheh, M., Amirian-Chakan, A., Triantafilis, J., 2019. Digital Mapping of Soil Classes Using Ensemble of Models in Isfahan Region, Iran. Soil Syst. 3, 37. https://doi.org/10.3390/soilsystems3020037.

Taghizadeh-Mehrjardi, R., Mahdianpari, M., Mohammadimanesh, F., Behrens, T., Toomanian, N., Scholten, T., Schmidt, K., 2020. Multi-task convolutional neural networks outperformed random forest for mapping soil particle size fractions in central Iran. Geoderma 376, 114552. https://doi.org/10.1016/j.geoderma.2020.114552.

Taylor, M.J., Smettem, K., Pracilio, G., Verboom, W., 2002. Relationships between soil properties and high-resolution radiometrics, central eastern Wheatbelt, Western Australia. Explor. Geophys. 33 (2), 95–102. https://doi.org/10.1071/EG02095.

Terraquest, L.T.D., 2009. Airborne horizontal gradient magnetic and radiometric survey, Centre region, France. BRGM.). BRGM, France. Operation report No. Operation report B-268.

Tifafi, M., Guenet, B., Hatté, C., 2018. Large Differences in Global and Regional Total Soil Carbon Stock Estimates Based on SoilGrids, HWSD, and NCSCD: Intercomparison and Evaluation Based on Field Data From USA, England, Wales, and France: Differences in total SOC stock estimates. Global Biogeochem. Cycles 32, 42–56. https://doi.org/10.1002/2017GB005678.

Tissoux, H., Prognon, F., Martelet, G., Tourlière, B., Despriée, J., Liard, M., Lacquement, F., 2017. Contribution of airborne gamma spectrometry to both characterisation and mapping of fluvial silico-clastic deposits in Loire valley and Sologne (Centre, France). Quaternaire 28, 87–103.

Vafaei Molamahmood, H., Qin, J., Yu, S., Long, M., 2021. Hydrogen peroxide decomposition into oxygen in different soils: Kinetic analysis, mechanism and implication in catalyzed hydrogen peroxide propagations. J. Clean. Prod. 304, 127116 https://doi.org/10.1016/j.jclepro.2021.127116.

Van Der Klooster, E., Van Egmond, F.M., Sonneveld, M.P.W., 2011. Mapping soil clay contents in Dutch marine districts using gamma-ray spectrometry. Eur. J. Soil Sci. 62, 743–753. https://doi.org/10.1111/j.1365-2389.2011.01381.x.

Vaysse, K., Lagacherie, P., 2015. Evaluating Digital Soil Mapping approaches for mapping GlobalSoilMap soil properties from legacy data in Languedoc-Roussillon (France). Geoderma Reg. 4, 20–30. https://doi.org/10.1016/j.geodrs.2014.11.003.

Vincent, S., Lemercier, B., Berthier, L., Walter, C., 2018. Spatial disaggregation of complex Soil Map Units at the regional scale based on soil-landscape relationships. Geoderma 311, 130–142. https://doi.org/10.1016/j.geoderma.2016.06.006.

Vos, C., Don, A., Prietz, R., Heidkamp, A., Freibauer, A., 2016. Field-based soil-texture estimates could replace laboratory analysis. Geoderma 267, 215–219. https://doi.org/10.1016/j.geoderma.2015.12.022.

Wadoux, A.-M.-J.-C., McBratney, A.B., 2021. Hypotheses, machine learning and soil mapping. Geoderma 383, 114725. https://doi.org/10.1016/j.geoderma.2020.114725.

Wadoux, A.-M.-J.-C., Minasny, B., McBratney, A.B., 2020a. Machine learning for digital soil mapping: Applications, challenges and suggested solutions. Earth Sci. Rev. 210, 103359 https://doi.org/10.1016/j.earscirev.2020.103359.

Wadoux, A.-M.-J.-C., Samuel-Rosa, A., Poggio, L., Mulder, V.L., 2020b. A note on knowledge discovery and machine learning in digital soil mapping. Eur. J. Soil Sci. 71, 133–136. https://doi.org/10.1111/ejss.12909.

Wetterlind, J., Richer-de-Forges, A.C., Nicoullaud, B., Arrouays, D., 2012a. Changes in uranium and thorium contents in topsoil after long-term phosphorus fertilizer application: U and Th after long-term P fertilizer application. Soil Use Manag. 28, 101–107. https://doi.org/10.1111/j.1475-2743.2011.00376.x.

Wetterlind, J., Tourliere, B., Martelet, G., Deparis, J., Saby, N., Richer-de-Forges, A.C., Arrouays, D., 2012b. Are there any effects of the agricultural use of chemical fertiliser on elements detected by airborne gamma-spectrometric surveys? Geoderma 173, 34–41. https://doi.org/10.1016/j.geoderma.2012.01.011.

Wilford, J., Minty, B., 2006. Chapter 16 The Use of Airborne Gamma-ray Imagery for Mapping Soils and Understanding Landscape Processes, in: Developments in Soil Science. Elsevier, pp. 207–610. https://doi.org/10.1016/S0166-2481(06)31016-1.

Wilford, J., 2002. Airborne gamma-ray spectrometry, in: Papp (Ed.), Geophysical and Remote Sensing Methods for Regolith Exploration, Open File Report, 144. Bertley, WA, Australia, pp. 46–52.

Zocatelli, R., Jacob, J., Gogo, S., Le Milbeau, C., Rousseau, J., Laggoun-Défarge, F., 2014. Spatial variability of soil lipids reflects vegetation cover in a French peatland. Org Geochem. 76, 173–183. https://doi.org/10.1016/j.orggeochem.2014.07.016.